# Low-Energy-Electron-Diffraction Spectra from [001] Surfaces of Face-Centered Cubic Metals: Theory and Experiment

D. W. Jepsen and P. M. Marcus
*IBM Thomas J. Watson Research Center, Yorktown Heights, New York* 10598

and

F. Jona*
*State University of New York, Stony Brook, New York* 11790
(Received 29 September 1971)

Extensive calculations of low-energy-electron-diffraction (LEED) spectra on face-centered cubic metals have been made with the layer-Korringa-Kohn-Rostocker (layer-KKR) method which treats multiple scattering within layers by the KKR method of band theory and multiple scattering between layers by matrix methods based on a beam representation of the wave field. The theory of the method is compactly and simply formulated using matrix notation. Calculations made with zero absorption in the material exhibit the close relationship in the structures of the curves for energy bands, reflected-flux spectra and transmitted-flux spectra, when plotted on a common energy scale. A check on the accuracy of the method is provided by the close agreement of the energy bands with independent calculations by standard methods. Calculations made with absorption for Al{001}, Cu{001}, and Ag{001} using 29 beams and 8 phase shifts for incident electrons up to 150 eV and for Al{001} at angles of incidence up to 25° are compared with experiment. A correction for lattice motion is introduced and several ways of matching waves at the surface are discussed. Detailed spectra at various angles show close correspondence between theory and experiment in relative peak positions, widths, and shapes and permit discrimination among crystal potentials. Estimates of inner potentials by comparison of measured and calculated spectra appear to provide information on the energy dependence of the effective one-electron potential in real crystal.

## I. INTRODUCTION

In a number of recent papers[1-5] the low-energy-electron-diffraction (LEED) spectra of Al{001} surfaces have been calculated in reasonable quantitative agreement with experiment, using several different one-electron potentials and a variety of methods. In a previous paper[1] we have used a potential which fits Fermi-surface data, supplemented by an imaginary part to describe inelastic scattering, and found a satisfactory fit to the positions and shapes of the spectral peaks out to electron energies of 150 eV for Al{001} at near-normal incidence. In this paper[6] we extend the calculations on Al{001} to other angles of incidence, add the correction for lattice motion, discuss the effects of various forms of surface matching, and compare theory and experiment for Cu{001} and Ag{001} using similarly constructed potentials.

We state briefly three useful conclusions which follow from our work and are discussed in more detail below: (i) the problem of diffraction of plane waves by a semi-infinite periodic solid with a realistic one-electron potential can be solved with sufficient accuracy to eliminate uncertainties in the calculation (leaving just the uncertainties in the potential); (ii) band-structure potentials (i.e., potentials that fit data on or near the Fermi surface), when supplemented as noted above, fit experimental LEED spectra surprisingly well up to the much higher energies of LEED experiments; (iii) comparison of theoretical and experimental LEED spectra permits an estimate of the energy dependence of the effective one-electron exchange-correlation potential in real crystals.

Our calculations are all carried out with a method conveniently referred to as the layer-KKR method,[7] which combines a treatment of multiple scattering in each layer by the Korringa-Kohn-Rostoker (KKR) method of band theory with our previously developed propagation matrix method[8] of handling multiple scattering between layers in a beam representation. We give a formulation of this method (Sec. II) in matrix-vector notation using the particularly simple analysis that follows the Korringa approach to KKR theory.[9] The analysis relies on expansions in plane and spherical waves and identities relating such expansions. The layer-KKR method draws upon the work of Kambe,[10] who developed the application of the KKR method to a single layer, and it is closely related to the method of Jennings and McRae,[11] who combined KKR for single layers with a matrix treatment of interlayer scattering. In our work, this basic two-step procedure is extended to complex potentials and carried through with a sufficient number of beams and phase shifts to provide an accurate solution to the LEED problem for a given potential at incident energies up to 150 eV.

Lack of agreement between measured and calculated spectra can therefore be related directly to inadequacies of the potential and the model of the surface (if not to errors in the measurement) but not to inaccuracies of calculation.

LEED spectra for Al{001} without absorption, i.e., with a real potential (the Snow self-consistent Hartree-Fock-Slater potential[12]), are calculated by the layer-KKR method in Sec. III in order to exhibit the close relationship of both reflection spectra (flux vs energy) and transmission spectra (flux into propagating Bloch functions vs energy) to the band structure—all plotted on a common energy scale. The results also exhibit the interconnection of the bands of Al along ⟨001⟩ by real lines. In addition the calculated bands have been satisfactorily checked against results found by standard methods of band-structure calculation.

Further tests against experiment of the Al{001} model used previously[1] are made in Sec. IV. This model introduces absorption by combining the Snow potential with an imaginary part taken from the work of Lundqvist[13] on the interacting uniform electron gas. LEED spectra are calculated over a series of polar angles up to 25°—but without the correction for lattice motion. The correspondence with measured spectra is rather good, although some discrepancies are noted, particularly at higher angles.

A simple procedure for averaging the scattering over lattice motion given by a Debye spectrum is carried out in Sec. V. The averaged matrix elements of the $t$ matrix of an individual atom are shown to depend on effective complex phase shifts which are given by an explicit sum over the original phase shifts (of the stationary atom) multiplied by a Debye-Waller factor. The resulting changes in the Al{001} spectra are shown to improve agreement with measured peak amplitudes.

Various methods of surface matching are described and compared in Sec. VI with the object of simulating the effect of the gradual variation of the potential between vacuum and crystal interior without detailed calculation of the transmission through the transition region. The different matching procedures do not change the spectra much, particularly at higher energies, but a method designated as the no-reflection method seems most suitable. This method leads beams through the transition region without reflection, but with appropriate refraction. The potential difference between vacuum and the inside of the crystal is determined by shifting calculated normal-incidence spectra along the energy axis to correspond best to measured spectra.

Averaging over lattice motion and matching by the no-reflection procedure are combined in Secs. VII and VIII with potentials for Cu and Ag that generate satisfactory band structures. LEED spectra are then calculated for the {001} faces of Al, Cu, and Ag and compared with experiment and with each other on a reduced plot to bring out the considerable variation of these spectra from each other. This variation is much greater than the difference between calculated and measured spectra in each case and arises from the considerable variation of the crystal potentials. The essential scattering properties of these potentials are given by the phase shifts and all of those used in the calculations are shown over the energy range of interest. The differences among Al, Cu, and Ag are brought out more clearly by a plot of the partial cross sections vs energy.

A discussion of the empirical energy shift required to bring calculated LEED spectra into correspondence with measured spectra is given in Sec. IX. The shift amounts to a determination of the average work function over the energy range of the spectra; from the fit over the range 30–150 eV the work function is found to be smaller than the static value. A plausible argument for just such a small work function is given from the known variation with energy of the effective one-electron exchange-correlation potential for a uniform interacting electron gas.[13] It is concluded that the careful analysis of LEED spectra may well provide useful information on the behavior of exchange-correlation potentials in a real crystal; also, that potentials which provide good band structures may work well over large energy ranges because the change with energy of exchange and correlation combined is rather small

## II. FORMULATION OF THE LAYER-KKR METHOD

The layer-KKR method has been discussed previously,[7] but the presentation there is lengthy and directed toward application to the band problem. It is useful to review the formulation here with particular emphasis on clarifying the basic ideas, simplifying the notation, and considering specifically the LEED application. We give a complete set of formulas on which the calculations are based, but not the detailed derivations for which we refer to our previous paper.

The method has a clear separation into two parts which will be discussed in turn: (i) the multiple-scattering problem between layers, including proper treatment of boundary conditions at the vacuum interface and at infinity in the bulk crystal, and (ii) multiple scattering between atomic scatterers in an elementary layer, i.e., a plane of atoms of one kind that is periodic in the infinite $\vec{\rho}$ plane ($\vec{\rho}$ is a two-dimensional position vector in the plane of the layer, perpendicular to the $z$ direction).

### Beam Representation of the Wave Field

Underlying the formulation is a special representation of the wave field which is particular suit-

able for surface problems (or slab problems which consist of a succession of layers of periodic media)—the beam representation.[14] In terms of this discrete representation, a very convenient vector-matrix notation can then be used to describe the wave field $\psi(\vec{r})$ and its transformations. Consider the expansion

$$\psi(\vec{r}) \equiv \psi(\vec{\rho}, z) \cong \sum_{n=1}^{N} \psi_n(z) p_n(\vec{\rho}), \tag{1}$$

$$p_n(\vec{\rho}) \equiv e^{i(\vec{k}_\rho + \vec{K}_{n\rho})\cdot\vec{\rho}}, \tag{2}$$

where $\psi(\vec{r})$ satisfies the Schrödinger equation $[\nabla^2 + E - V(\vec{r})]\psi(\vec{r}) = 0$ in the given potential $V(\vec{r})$ which describes the layered structure and may be complex; $\vec{K}_{n\rho}$ is the $n$th reciprocal-lattice vector of the two-dimensional lattice or net in the plane at $z$, $\vec{k}_\rho$ is a given component of wave number in the $\vec{\rho}$ plane corresponding to the incoming wave, and $E$ is the energy ($\vec{k}_\rho$ and $E$ characterize the incident electron and the entire wave field). Thus $\psi(\vec{r})$ at any $z$ is expanded in a two-dimensional Fourier series in the $\vec{\rho}$ plane which is cut off after $N$ terms.

If the wave field is in a vacuum, $\psi_n(z)$ may be uniquely expressed as the sum of two running (or attenuating) waves with constant amplitudes $\alpha_n^+$ and $\alpha_n^-$ for waves toward $+z$ (the right) and $-z$ (the left), respectively:

$$\psi_n(z) = \alpha_n^+ e^{ik_{nz}z} + \alpha_n^- e^{-ik_{nz}z} \equiv \varphi_n^+(z) + \varphi_n^-(z), \tag{3}$$

$$k_{nz} = [E - (\vec{k}_\rho + \vec{K}_{n\rho})^2]^{1/2}. \tag{4}$$

Thus $\psi(\vec{\rho}, z)$ in vacuum is expanded in a special set of $2N$ plane waves or beams which all have the same energy and reduced component of wave number in the $\vec{\rho}$ plane. By opening an infinitesimal slot inside the crystal at any plane $z$, we find that this same form for $\psi_n(z)$ is obtained in the slot; hence (3) applies everywhere in the crystal, but now $\alpha_n^+$ and $\alpha_n^-$ are functions of $z$.

### Multiple Scattering between Layers and the $\underline{Q}$ Matrix

In the beam representation $\psi(\vec{r})$ can be compactly designated by the $2N$ component vectors $\underline{\Phi}(z)$ or $\underline{\alpha}(z)$ defined by

$$\underline{\Phi}(z) = \begin{pmatrix} \underline{\varphi}^+(z) \\ \underline{\varphi}^-(z) \end{pmatrix} = \begin{pmatrix} \vdots \\ \alpha_n^+(z)\, e^{ik_{nz}z} \\ \vdots \\ \alpha_n^-(z)\, e^{-ik_{nz}z} \\ \vdots \end{pmatrix} = \begin{pmatrix} \ddots & & & \\ & e^{ik_{nz}z} & 0 & \\ & & \ddots & \\ & 0 & & e^{-ik_{nz}z} \\ & & & \ddots \end{pmatrix} \begin{pmatrix} \vdots \\ \alpha_n^+(z) \\ \vdots \\ \alpha_n^-(z) \\ \vdots \end{pmatrix} \equiv \underline{D}(z)\, \underline{\alpha}(z)\,. \tag{5}$$

Note that $\underline{\Phi}(z)$ and $\underline{\alpha}(z)$ are continuous at any $z$, including interfaces between crystals or with vacuum. Consider the relation between the wave field vectors $\underline{\Phi}(z_-)$ and $\underline{\Phi}(z_+)$ at the left and right sides of a layer. These vectors must be linearly related by a matrix $\underline{Q}$ (the transfer matrix) because of the linearity of the differential equation for $\psi(\vec{r})$,

$$\underline{\Phi}(z_+) = \underline{Q}\,\underline{\Phi}(z_-)\,. \tag{6}$$

Then $\underline{Q}$ describes the effects of the given layer on the wave field for all conditions of incident fields; $\underline{Q}$ will be related later to a scattering matrix for the layer, but now we assume it is known. If the crystal is made up of repetitions of the layer giving rise to $\underline{Q}$, then eigenvectors of $\underline{Q}$ describe characteristic modes of the crystal, since the corresponding $\psi(\vec{r})$ repeats with a constant factor on translating through one layer; the modes may also be called generalized Bloch functions, generalized to allow the magnitude of the constant factor to differ from unity. Introducing $\underline{\mathfrak{B}}$, the ordered-column matrix of $\underline{Q}$, ordered so that the first $N$ columns propagate or attenuate toward $+z$ and the second $N$ toward $-z$, we have

$$\underline{Q}\,\underline{\mathfrak{B}} = \underline{\mathfrak{B}}\,\underline{\Lambda}\,, \tag{7}$$

where the eigenvalue matrix $\underline{\Lambda}$ is a diagonal matrix with elements $e^{ik_z a}$ containing the thickness $a$ of the repeating layer and the $k_z$ values of the various Bloch waves ($k_z$ can be complex in general). Now any $\underline{\Phi}(z)$ can be resolved into Bloch waves with an amplitude vector $\underline{\gamma}$ (independent of $z$) in the form

$$\underline{\Phi}(z) = \underline{\mathfrak{B}}\,\underline{\gamma}\,. \tag{8}$$

Note that (5) shows that $\underline{D}(z)$ is the Bloch wave matrix of the vacuum.

If the crystal is semi-infinite (extending toward $+z$), then no Bloch waves come in from infinity and (the transpose of) $\underline{\gamma}$ has the form $(xx\cdots x00\cdots 0)$; i.e., the last $N$ components of $\underline{\gamma}$ vanish. The matching conditions at a vacuum-crystal interface at $z = z_0$ are then

$$\underline{\Phi}(z_0) = \underline{D}(z_0)\,\underline{\alpha}(z_0) = \underline{\mathfrak{B}}(z_0)\,\underline{\gamma} \tag{9}$$

or, in terms of the unit amplitude of one incident wave, $N$ unknown reflection coefficients $\mathfrak{R}_n$, $N$ unknown transmission coefficients into Bloch waves $\mathcal{T}_n$, (9) gives $2N$ equations in $2N$ unknowns,

$$\underline{\mathfrak{B}}^{-1}(z_0)\underline{D}(z_0) \begin{pmatrix} 1 \\ 0 \\ \cdot \\ \cdot \\ \cdot \\ 0 \\ \mathfrak{R}_1 \\ \cdot \\ \cdot \\ \cdot \\ \mathfrak{R}_N \end{pmatrix} = \begin{pmatrix} \mathcal{T}_1 \\ \cdot \\ \cdot \\ \cdot \\ \mathcal{T}_N \\ 0 \\ \cdot \\ \cdot \\ \cdot \\ 0 \end{pmatrix} . \tag{10}$$

Finally, we note that a scattering matrix for a layer can be defined by the linear relation between incoming waves and outgoing waves on the left and the right:

$$\underline{\Phi}^{\text{out}} \equiv \begin{pmatrix} \underline{\varphi}^{+}(z_+) \\ \underline{\varphi}^{-}(z_-) \end{pmatrix} = \underline{S} \begin{pmatrix} \underline{\varphi}^{+}(z_-) \\ \underline{\varphi}^{-}(z_+) \end{pmatrix} \equiv \underline{S}\,\underline{\Phi}^{\text{in}} , \tag{11}$$

where $\underline{\phi}^{\pm}(z)$ are the $N$-component vectors defined in (5). Now comparing (11) and (6) gives

$$\underline{Q} = \begin{pmatrix} \underline{S}_{11} - \underline{S}_{12}\underline{S}_{22}^{-1}\underline{S}_{21} & \underline{S}_{12}\underline{S}_{22}^{-1} \\ \underline{S}_{22}^{-1}\underline{S}_{21} & \underline{S}_{22}^{-1} \end{pmatrix} , \tag{12}$$

where $\underline{S}_{11}$ is the upper-left $N\times N$ quadrant of $\underline{S}$, etc.

### Multiple Scattering in a Layer and the $\underline{S}$ Matrix

For this paper we restrict attention to a single layer of thickness $a$ containing a two-dimensional periodic array (Bravais net) of nonoverlapping, spherically symmetric, scattering potentials, each of finite radius less than $\frac{1}{2}a$ and centered on the midplane of the layer; between the spheres the potential is constant. This scattering object will be referred to as an elementary layer with a muffin-tin potential made up of an array of atomic potentials, each in the center of a cell. At $z_-$ and $z_+$, the left and right boundaries of the layer, (hence $z_+ - z_- = a$) the wave field is given in the beam representation by the vectors $\underline{\Phi}(z_-)$ and $\underline{\Phi}(z_+)$, or by the mixed beam vectors $\underline{\Phi}^{\text{in}}$ and $\underline{\Phi}^{\text{out}}$ as in (11). Then $\underline{\Phi}^{\text{in}}$ determines the entire field structure including $\underline{\Phi}^{\text{out}}$ and the problem is to find the matrix $\underline{S}$ which transforms $\underline{\Phi}^{\text{in}}$ into $\underline{\Phi}^{\text{out}}$. For this potential, it is convenient to define the beam representation slightly differently by replacing Eq. (4) by $k_{nz} = [E - V_0 - (\vec{k}_\rho + \vec{K}_{n\rho})^2]^{1/2}$ where $V_0$ is the complex constant potential between atoms (imaginary part $-i\beta$).

The essential element in the analysis is to transform the beam representation into a spherical-wave representation in which the scattering can be accurately calculated by using the phase shifts of the potential at each atomic center and then to transform back to the beam representation. The analytical tools required for these transformations are various identities giving expansions in spherical waves. The development given here will be along the lines introduced by Korringa in his formulation of the KKR method[9] in which the wave field is resolved into incident and scattered waves, but now carried out for a layer with plane waves incident upon it.

It will be convenient to introduce a second origin at the center of one atomic potential in the layer (the reference center) whose position vector with respect to the first origin is $\vec{r}_0$ and to systematically use primed notation for position coordinates with respect to the reference center; hence, we introduce

$$\vec{r}' = \vec{r} - \vec{r}_0, \quad \vec{r} \equiv (\vec{\rho}, z), \quad \vec{r}_0 \equiv (\vec{\rho}_0, z_0), \quad \vec{r}' \equiv (\vec{\rho}', z') ,$$

$$\vec{\rho}' = \vec{\rho} - \vec{\rho}_0, \quad z' = z - z_0, \quad z_0 = z_\mp \pm \tfrac{1}{2}a .$$

Now introduce the asymptotic spherical-wave expansion for $\psi(\vec{r})$ around the reference center and in the reference cell (which holds on the sphere and in some range outside it) in the form

$$\psi(\vec{r}') = \sum_L [A_L \mathcal{J}_L(\vec{r}') + B_L \mathcal{K}_L(\vec{r}')] , \tag{13}$$

$$\mathcal{J}_L(\vec{r}') \equiv i^l Y_{lm}(\vec{r}') j_l(kr') , \tag{14}$$

$$\mathcal{K}_L(\vec{r}') \equiv i^{l+1} Y_{lm}(\vec{r}') h_l(kr') , \tag{15}$$

where $L$ enumerates the pairs of indices $l$ and $m$, the $Y_{lm}$ are spherical harmonics, $j_l(kr')$ is the spherical Bessel function of the first kind, $h_l(kr')$ the outgoing-wave spherical Bessel function—both of order $l$, and $k = (E - V_0)^{1/2}$. Note $\mathcal{J}_L(\vec{r}')$ and $\mathcal{K}_L(\vec{r}')$ are spherical waves belonging to a particular $E$ or $k$, and implicitly contain this variable. There will be a maximum value of $L$ required in the calculation which will be denoted $\mathcal{L}$. The value of $\mathcal{L}$ will be determined by the largest non-negligible phase shift $\eta_l$. Then if the higher phase shifts were strictly zero, with this $\mathcal{L}$ there would be no approximation in cutting off the series (13). [This can be seen from the vanishing of the elements of $\underline{D}''$ in (29) when $\eta_l$ vanishes; hence, the corresponding part of $\underline{S}$ in (38) vanishes.]

From (13), $\psi(\vec{r})$ is determined throughout the layer by the Bloch relations

$$\psi(\vec{r} + \vec{R}_j) = e^{i\vec{k}_\rho \cdot \vec{R}_j}\,\psi(\vec{r}) , \tag{16}$$

where $\vec{R}_j$ is a two-dimensional lattice vector of the layer. In (13) the terms in $B_L$ and $A_L$, which can be regarded as components of vectors $\underline{B}$ and $\underline{A}$, describe, respectively, the separation of $\psi$ in the

reference cell into outgoing spherical waves scattered by the atomic potential at $\vec{r}' = 0$, and incident spherical waves coming from other sources (outside the cell). Now we can proceed in three stages to relate $\underline{\Phi}^{in}$ to $\underline{\Phi}^{out}$: first by relating $\underline{A}$ to $\underline{\Phi}^{in}$ and $\underline{B}$ through a decomposition of $\underline{A}$ into contributions from outside and inside the layer; second by relating $\underline{B}$ to $\underline{A}$ through the scattering phase shifts; third by relating $\underline{\Phi}^{out}$ to $\underline{\Phi}^{in}$ and $\underline{B}$ by forming the outgoing plane waves as the sum of contributions from incident plane waves (on the layer) and scattered waves from all the atomic centers in the layer. Then eliminating $\underline{A}$ and $\underline{B}$ among these three linear relations gives the desired relation for $\underline{S}$.

The first stage in the derivation of $\underline{S}$ establishes the relation

$$\underline{A} = \underline{U}\,\underline{\Phi}^{in} + \underline{V}\,\underline{B} . \tag{17}$$

The $\mathfrak{L}\times 2N$ rectangular matrix $\underline{U}$ is obtained by transforming the incident plane waves into spherical wave expansions in $\mathcal{J}_L(\vec{r}')$, showing they contribute to $\underline{A}$. First, the general components of the incident plane waves from the left and right are rewritten in the form

$$\varphi_n^{\pm}(z)\,p_n(\vec{\rho}) \equiv \varphi_n^{\pm}(z_{\mp})\,p_n(\vec{\rho}_0)\,e^{ik_{n\perp}a/2}\,e^{i\vec{k}_n^{\pm}\cdot(\vec{r}-\vec{r}_0)} , \tag{18}$$

$$\vec{k}_n^{\pm} \equiv (\vec{k}_\rho + \vec{K}_{n\rho},\ \pm k_{n\perp}) , \tag{19}$$

which expresses each component in terms of its value on the layer boundaries $z_\pm$ and at a definite value of $\vec{\rho}(=\vec{\rho}_0$ the position of the reference center), multiplied by a phase factor $e^{ik_{n\perp}a/2}$ and by a plane wave $e^{i\vec{k}_n^{\pm}\cdot\vec{r}'}$. The latter may be expanded in spherical waves in $\vec{r}'$ by the identity

$$e^{i\vec{k}_n^{\pm}\cdot\vec{r}'} = 4\pi\textstyle\sum_L Y_L(\vec{k}_n^{\pm})\,\mathcal{J}_L(\vec{r}'), \quad |\vec{k}_n^{\pm}| = k \tag{20}$$

where the condition on $|\vec{k}_n^{\pm}|$ follows from (19) and (4). Since the constant potential $V_0$ between the atomic potentials is generally complex, the quantities $k = (E - V_0)^{1/2}$ and $k_{n\perp}$ are generally complex, and even when $V_0$ is real, $k_{n\perp}$ for large $\vec{K}_{n\rho}$ is imaginary. However, the formulas still hold; in particular the $Y_{lm}(\vec{k}_n^{\pm})$ can be calculated as polynomials in the (complex) components of the unit vector $\vec{k}_n^{\pm}/k$. Note that $|\vec{k}_n^{\pm}|$ means the magnitude of the vector $\vec{k}_n^{\pm}$ with complex components and is in general complex $(=k)$. Thus the incident wave vectors $\varphi^+(z_-)$ and $\varphi^-(z_+)$ [see (11)] give rise to spherical waves $\mathcal{J}_L(\vec{r}')$ in the reference cell whose coefficients give the matrix $\underline{U}$ in the form

$$\underline{U} = 4\pi\,\underline{Y}\underline{D}'(\tfrac{1}{2}a) . \tag{21}$$

In (21), $\underline{Y}$ is an $\mathfrak{L}\times 2N$ matrix whose elements are

$$Y_{Ln} = Y_L(\vec{k}_n^{+}), \quad Y_{L,n+N} = Y_L(\vec{k}_n^{-}),$$
$$L = 1 \text{ to } \mathfrak{L}, \qquad n = 1 \text{ to } N \tag{22}$$

and $\underline{D}'(a/2)$ is a $2N\times 2N$ diagonal matrix which supplies the phase factors $e^{ik_{n\perp}a/2}$ in (18); $\underline{D}'(z)$ has elements

$$D'_{mn}(z) = D_{m+N,n+N}(z) = e^{ik_{n\perp}}\delta_{mn} , \tag{23}$$

where $\delta_{mn} = 0$ unless $m = n$ and $\delta_{nn} = 1$. Note $\underline{D}'(z) \neq \underline{D}(z)$ because the lower $N$ elements in $\underline{D}'(z)$ are the same as the first $N$.

The $\mathfrak{L}\times\mathfrak{L}$ matrix $\underline{V}$ is obtained by summing the outgoing spherical waves $B_L\,\mathcal{H}_L(\vec{r}' - \vec{R}_j)$ from all the other atomic centers at the positions $\vec{R}_j \neq 0$, but with the proper relative phase factor $e^{i\vec{k}_\rho\cdot\vec{R}_j}$ determined by the Bloch property (16). This sum is converted to an expression in $\vec{r}'$ by the identity

$$\mathcal{H}_L(\vec{r}' - \vec{R}) = 4\pi \sum_{L_1,L_2} C_{LL_1L_2}\mathcal{H}_{L_1}(-\vec{R})\,\mathcal{J}_{L_2}(\vec{r}'), \quad |\vec{R}| > |\vec{r}'| \tag{24}$$

where the Gaunt coefficients $C_{LL_1L_2}$ are given by

$$C_{LL_1L_2} \equiv \int_{4\pi} Y_L(\vec{k})\,Y_{L_1}(\vec{k})\,Y_{L_2}(\vec{k})\,d^2\Omega_k . \tag{25}$$

The result of using (24) in the sum and picking out the coefficient of $\mathcal{J}_L(\vec{r}')$ is to determine the elements of the $\mathfrak{L}\times\mathfrak{L}$ matrix $\underline{V}$ in the form

$$V_{LL_2} = -4\pi \sum_{L_3=1}^{\mathfrak{L}} C_{LL_2L_3}\mathfrak{D}_{L_3} , \tag{26}$$

$$\mathfrak{D}_L \equiv -\textstyle\sum_j' e^{i\vec{k}_\rho\cdot\vec{R}_j}\mathcal{H}_L(-\vec{R}_j), \quad j \neq 0 . \tag{27}$$

The second stage in the derivation of $\underline{S}$ introduces the relation between $B_L$ and $A_L$ in terms of the phase shifts $\eta_l$ of each spherical atomic-scattering potential

$$\underline{B} = \underline{D}''\,\underline{A} , \tag{28}$$

where $\underline{D}''$ is a constant diagonal matrix with elements

$$D''_{L,L_2} = \delta_{L_1L_2}/(\cot\eta_l - i) = \delta_{L_1L_2}e^{i\eta_l}\sin\eta_l . \tag{29}$$

The third stage in the derivation of $\underline{S}$ establishes the relation

$$\underline{\Phi}^{out} = \underline{D}'(a)\,\underline{\Phi}^{in} + \underline{W}\,\underline{B} . \tag{30}$$

In (30), $\underline{D}'(a)$ is the diagonal $2N\times 2N$ matrix defined in (23) which introduces the correct phase change to convert the components of $\underline{\Phi}^{in}$, namely, $\underline{\varphi}^+(z_-)$ and $\underline{\phi}^-(z_+)$, to the components of $\underline{\Phi}^{out}$, namely $\underline{\phi}^+(z_+)$ and $\underline{\phi}^-(z_-)$, respectively. Obtaining $\underline{W}$, like $\underline{V}$, requires summing the outgoing waves from the atomic centers with proper phases $B_L\,\mathcal{H}_L(\vec{r}' - \vec{R}_j)\,e^{i\vec{k}_\rho\cdot\vec{R}_j}$ but, unlike $\underline{V}$, now all centers are summed over (including $\vec{R}_j = 0$) and the sum is to be expressed in the plane-wave basis at $z = z_+$ and $z_-$ required for $\underline{\Phi}^{out}$. This sum is contained in the expansion of Green's function $G(\vec{r}')$ for the layer, i.e., the solution of

the Schrödinger equation in vacuum for energy $E$ and wave number component $\vec{k}_\rho$ in the presence of unit $\delta$-function sources at the atom centers $\vec{R}_j$, which has the well-known form[10]

$$G(\vec{r}\,') = -\frac{1}{4\pi}\sum_j \frac{\exp(ik|\vec{r}\,'-\vec{R}_j| + i\vec{k}_\rho\cdot\vec{R}_j)}{|\vec{r}\,'-\vec{R}_j|} \quad . \tag{31}$$

Each term of (31) can be expanded in spherical waves in $\vec{r}\,'$ by means of the identity

$$e^{ik|\vec{r}_1'+\vec{R}|}/k|\vec{r}_1'+\vec{R}| = 4\pi\sum_L \mathcal{J}_L(\vec{r}_1')\mathcal{H}_L(\vec{R}) \ , \quad |\vec{R}| > |\vec{r}_1'| \ . \tag{32}$$

In (32) put $\vec{r}_1' = \vec{r}\,' - \vec{r}_{2\pm}'$ and take $\vec{r}_{2\pm}' \equiv (\vec{\rho}_2', z_{2\pm}') = (\vec{\rho}_2', \pm\frac{1}{2}a)$; hence, $\vec{r}_{2\pm}'$ is on the layer boundaries (as desired for $\Phi^{\text{out}}$). Take $\vec{r}_1'$ within the reference atomic potential, and take $\vec{R} = \vec{r}_{2\pm}' - \vec{R}_j$; hence, $|\vec{R}| > |\vec{r}_1'|$ [so that the required inequality in (32) is satisfied]; then, using (32) with these substitutions, (31) becomes

$$G(\vec{r}_1' + \vec{r}_{2\pm}') = -k\sum_L \mathcal{J}_L(\vec{r}_1')\sum_j e^{i\vec{k}_\rho\cdot\vec{R}_j}\mathcal{H}_L(\vec{r}_{2\pm}' - \vec{R}_j) \ , \tag{33}$$

which contains the desired sums.

Now express $G(\vec{r}\,')$ in the beam representation[10,14] as a sum of beams (i.e., plane waves with the same energy $E$) chosen to satisfy outgoing-wave conditions at $z' = \pm\infty$, and with a proper discontinuity (in slope) at $z' = 0$. This gives

$$G(\vec{r}\,') = (1/2i\mathcal{A})\sum_n e^{ik_{nz}|z'|}p_n(\vec{\rho}\,')/k_{nz} \ , \tag{34}$$

where $\mathcal{A}$ is the area of a unit cell of the net of $\vec{R}_j$'s. Again as in (32) putting $\vec{r}\,' = \vec{r}_1' + \vec{r}_{2\pm}'$, hence $|z_1' + z_2'| = \frac{1}{2}a \pm z_1'$, and noting the factors $e^{\pm ik_{nz}z'}p_n(\vec{\rho}_1') = e^{i\vec{k}_n^{\pm}\cdot\vec{r}_1'}$ can be expanded using (20), then (34) becomes

$$G(\vec{r}_1' + \vec{r}_{2\pm}') = (2\pi/i\mathcal{A})\sum_L \mathcal{J}_L(\vec{r}_1') \times\sum_n e^{ik_{nz}a/2}Y_L(\vec{k}_n^{\pm})p_n(\vec{\rho}_2')/k_{nz} \ . \tag{35}$$

Comparison of the coefficients of $\mathcal{J}_L$ in (33) and (35) evaluates the $2N\times\mathfrak{L}$ matrix $\underline{W}$ in the form

$$\underline{W} = (2\pi i/k\mathcal{A})\,\underline{D}'(a/2)\,\underline{\mathcal{K}}^{-1}\,\underline{\tilde{Y}} \ , \tag{36}$$

where $\underline{\tilde{Y}}$ is the transpose of $\underline{Y}$ defined in (22), $\underline{D}'(z)$ is defined in (23), and $\underline{\mathcal{K}}^{-1}$ is the diagonal matrix with elements

$$\mathcal{K}_{mn}^{-1} = \mathcal{K}_{m+N,n+N}^{-1} = \delta_{mn}/k_{nz}, \quad m,n = 1 \text{ to } N \ . \tag{37}$$

Finally, combining (17), (21), (28), (30), (36) and eliminating $\underline{A}$ and $\underline{B}$ gives

$$\underline{S} = \underline{D}'(a) + (8\pi^2 i/k\mathcal{A})\,\underline{D}'(a/2)\,\underline{\mathcal{K}}^{-1} \times \underline{\tilde{Y}}((\underline{D}'')^{-1} - \underline{V})^{-1}\,\underline{Y}\underline{D}'(a/2) \ , \tag{38}$$

where formulas for the matrix elements of $\underline{D}'$, $\underline{\mathcal{K}}^{-1}$, $\underline{Y}$, $\underline{D}''$, and $\underline{V}$ are given in (23), (37), (22), (29), and (26), respectively. We can easily understand qualitatively the significance of the terms which made up $\underline{S}$ in (38) and convert the incident field into the outgoing field. Starting from the right, $\underline{D}'(a/2)$ operates on the field of incident plane waves to shift their phase to the midplane of the layers; $\underline{Y}$ then transforms the field into stationary spherical waves around the atom centers, $(\underline{D}''^{-1} - \underline{V})^{-1}$ transforms stationary spherical waves into outgoing spherical waves, $\underline{\mathcal{K}}^{-1}\underline{\tilde{Y}}$ transforms outgoing spherical waves into outgoing plane waves, $\underline{D}'(a/2)$ shifts the phase from the midplane on to the boundaries of the layer, and $\underline{D}'(a)$ adds the incident waves after they have been shifted in phase through the full layer thickness to give the total outgoing plane-wave field. The calculation of reflection coefficients $\mathcal{R}_n$ and relative fluxes $(k_{nz}/k_{1z})|\mathcal{R}_n|^2$ now follows from $\underline{S}$ by finding $\underline{Q}$ from $\underline{S}$ using (12), $\mathcal{B}$ from $\underline{Q}$ by solving the eigenvalue equation (7), and the $\mathcal{R}_n$ from the linear equation (10). Details of the numerical procedure for evaluation of these various quantities will not be discussed here.

## III. BAND STRUCTURE AND LEED SPECTRA WITHOUT ABSORPTION

Although absorption and lattice motion produce similar marked effects on the character of LEED spectra, we first exhibit the spectra calculated without these complications for two reasons—as a test of the method of calculation and to indicate clearly by comparison the changes produced by absorption and lattice motion. The calculations are somewhat more difficult without absorption because it is more complicated to determine which Bloch functions carry flux into the crystal, and because the spectra show much fine structure which requires calculations at much more closely spaced intervals than with absorption. However, the effect of absorption on the Ewald procedure we use is small, whereas methods which depend on absorption to sum the multiple-scattering series do not work in the no-absorption limit. The correctness and accuracy of the computation program will be tested by comparison of the energy bands, which are generated in the course of the LEED calculation (from eigenvalues of the $\underline{Q}$ matrix), with the results of various standard procedures for solving the band problem in a bulk crystal. We also obtain solutions to the band problem corresponding to attenuating waves, which are difficult to obtain from the usual band-structure calculation procedures, but play an important role in surface problems. We show the real lines corresponding to these solutions in Fig. 1.

The LEED calculation has been carried out on Al{001} at normal incidence over the energy range

0–70 eV using the Snow potential[12] with no imaginary part ($\beta = 0$) and a simple boundary condition at the surface (chosen halfway between neighboring planes of atoms) which takes the vacuum level at the muffin-tin reference level, i.e., no discontinuity at the surface on proceeding from vacuum into the space between the scattering spheres. The results of the calculation are shown in the six plots of Fig. 1 which share a common energy scale; in particular, the band structure is plot 4 (from the top) shown along the $\Delta$ line ($\Gamma$ at the top, $X$ at the bottom) with a reduced $k_z$ scale. The bands are shown supplemented by the real lines between band edges—actually by the projected real lines, since the quantity plotted as a function of $E$ is the real part of the complex $k_z$ for which $E$ remains real between bands. The visible projected real lines in the plot start from band edges inside the Brillouin zone, e.g., from 42 to 45 eV at $k_z a/\pi \simeq 0.8$, but there are also projected real lines along the energy axes at $\Gamma$ and $X$ which are not shown, e.g., from 5 to 7 eV along the axis at $X$, and also one from 14 eV to $-\infty$.

Plot 5 provides a complementary view of the real lines, namely, their projection on the imaginary $k_z$ and $E$ plane, where the reduced scale of $k_z$ is such that at the value $-1$ the square of the corresponding attenuating Bloch wave is reduced by a factor 10 in a distance $a$. The real lines from the view of plot 5 are either tight loops joining band edges, e.g., from 5 to 7 eV—although sometimes loops will merge, as occurs at 28 eV—or they are half-loops arcing down to $E = -\infty$ but quickly crossing the line of maximum attenuation in the diagram. These half-loops easily identify the start of each new band, showing that eight or nine new bands (some degenerate) start over the 70-eV range of the plot (the apparent half-loops starting at 63 eV appear to be part of large closed loops). Each new band, once started, actually may be traced continuously to $E = +\infty$ by using real lines to bridge the energy gaps. The uniqueness of the continuation is shown more clearly by adding a small amount of absorption, whereupon the distinction between bands and real lines is wiped out since $k_z$ is always complex. The projected real lines in the band gaps of plot 4 then each split into two parts which join continuously—the lower part of the left band (the part up to the band edge) with the upper part of the right band and vice versa.

The actual magnitudes of the energy bands have been compared with the calculations by Connolly[15] with the augmented-plane-wave method and the identical potential[12] for Al. Careful comparison of plot 4 with Connolly's shows that the two plots are very close.[16] The calculated energies have also been checked by comparison of a few pairs of $E, k_z$ values with results of a standard KKR band-structure program.[17] Agreement is found to within 0.1%, the accuracy of the KKR calculation. Finally, the $E, \vec{k}$ pairs have been used to make a valuable check on the formulation of the method as well as on the calculation program by comparing the same $E$ and $\vec{k}$ pairs using separate LEED calculations for the $\{001\}$ and the $\{111\}$ surfaces. All the detailed matrix elements are now different, but the results for $\vec{k}$ at the same $E$ agree to 0.002%.

The LEED spectra obtained from the complete Al$\{001\}$, $\theta = 0°$, LEED calculation, which requires the Bloch functions as well as the band energies, are shown in plots 1, 2, 3 and 6. The reflection spectra for the 00, 11, and 20 beams show sharp

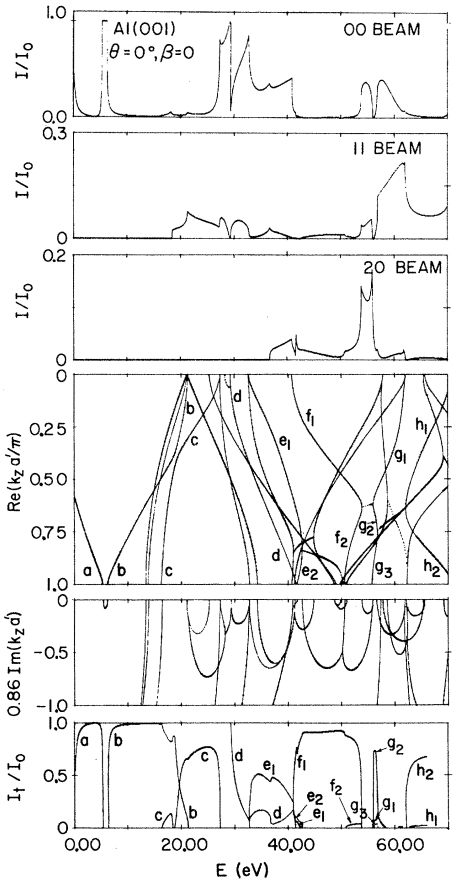


FIG. 1. Band structure, reflection and transmission spectra on a common energy scale from 0 (vacuum level) to 70 eV for Al$\{001\}$. Calculation assumes no absorption ($\beta = 0$), normal incidence ($\theta = 0$), the Snow potential (Ref. 12), muffin-tin zero at vacuum level (no step), no shift of spectra along energy scale. Plots 1 to 3: reflected flux relative to incident flux for 00, 11, 20 beams. Plot 4: band structure along [001] with real part of real line dotted and bands of $\Delta_1$ symmetry marked. Plot 5: imaginary part of real line. Plot 6: transmitted flux into Bloch waves relative to incident flux, marked to correspond to bands of plot 4. $a' = a/2$ = period in the $z$ direction.

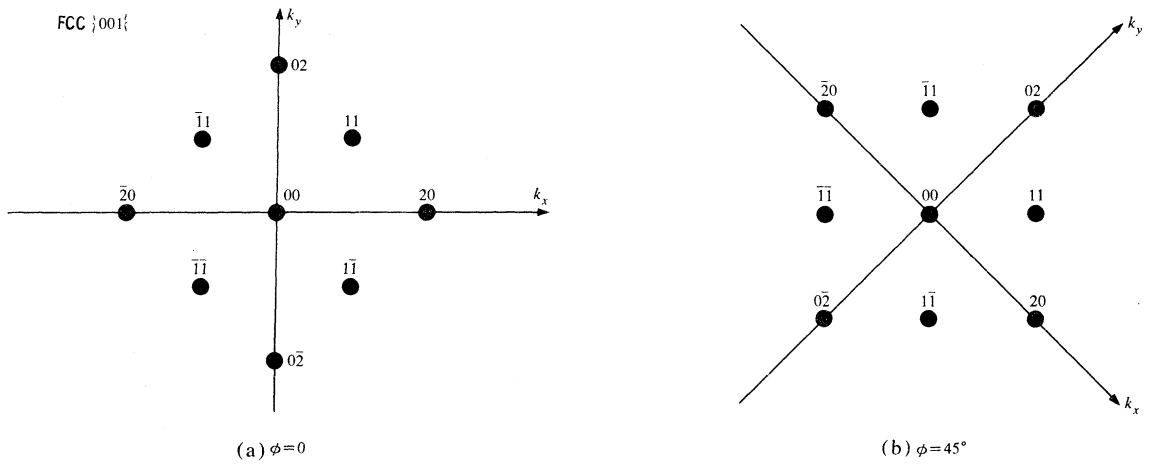


FIG. 2. Schematic LEED pattern from {001} surface of fcc crystal with pertinent indexing of beams for azimuth angle $\phi = 0°$ [diagram (a)] and 45° [diagram (b)]. The plane of incidence in each case passes through a horizontal axis. The pattern moves to the right as $\theta$ is increased.

structure—steep rises, sharp corners and peaks, deep dips (i.e., to very small magnitudes)—which correlate closely with each other and with features of the band structure, such as steep rises occurring in the vicinity of band edges. Only bands of $\Delta_1$ symmetry (marked by letters $a$ to $h$ in Fig. 2) are significant because the incident electron strikes the surface normally and contributions from other bands are forbidden. The excitation of various bands is most easily seen in the transmission spectrum of plot 6 which gives the flux carried by all propagating Bloch functions at any energy. The same letters which mark the $\Delta_1$ bands in plot 4 are used for the corresponding transmitted-flux values in plot 6. This plot shows vividly the division of flux among the $\Delta_1$ Bloch waves at any energy. There is some flux in every $\Delta_1$ line, but one band usually has most of the flux, except near band edges of overlapping bands where one band dies out and the other rises, e.g., around 20 eV where flux in band $b$ transfers to band $c$, around 33 eV where flux in band $d$ transfers mainly but not entirely to band $e_1$, and then around 42 eV flux in $e_1$ is transferred mainly to new band $f_1$, but also slightly to $e_2$ (the part of $e$ on the lower side of the band edge at 42.5 eV). Note that narrow band $g$ supplies three propagating Bloch functions in a narrow energy range around 56.5 eV, all excited. One can trace a path of strong excitation through plot 4 in the sequence $a$, lower $b$, upper $c$, upper $d$, $e_1$, $f_1$, $g_2$, $h_2$ resembling a broken-up free-electron 00 band. Note that the transmission spectra also show features associated with the free-electron band structure, such as the sudden sharp dip in amplitude of band $c$ at 18 eV when the 11 beam starts to propagate (in vacuum), or in band $e$ at 37 eV when the 20 beam starts propagating.

In actual crystals, the presence of absorption, besides strongly reducing the intensities, smooths out the sharp features, rounds the peaks and corners, and fills in the deep dips in the LEED spectra. Absorption also substantially changes the appearance of the band structure, since every $k_z$ now has some imaginary part and all bands may now cross each other on the plots of $E$ vs the real part of $k_z$. For high absorption these band plots (i.e., projected real lines) look free-electron-like. Peaks in the reflected LEED spectra still correlate with the crossings of bands but the band plots, particularly at higher energies, can be too complicated to give much insight into the LEED spectra directly.

No precise check on the LEED spectra against independent calculations is available as was possible for the energies. However, an internal check on the precision of the calculation is provided by the test of flux conservation: The total incident flux is found to equal the flux of reflected propagating beams plus the flux transmitted into propagating Bloch waves to seven or eight figures (16 figures are carried in all operations).

## IV. LEED SPECTRA WITH ABSORPTION AT VARIOUS ANGLES OF INCIDENCE FOR Al {001}

The Snow potential for Al used in Sec. III has been fairly successful[1,18] in fitting observed LEED spectra for Al{001}, when augmented by an imaginary part of 0.3 Ry (4.1 eV) to describe absorption, and used with no discontinuity (in the real part of the potential) at the surface to avoid the unphysically high reflection produced by a sharp step. The calculated spectra are then shifted down in energy by 7.5 eV to match experiment—which amounts to an empirical determination of the work function

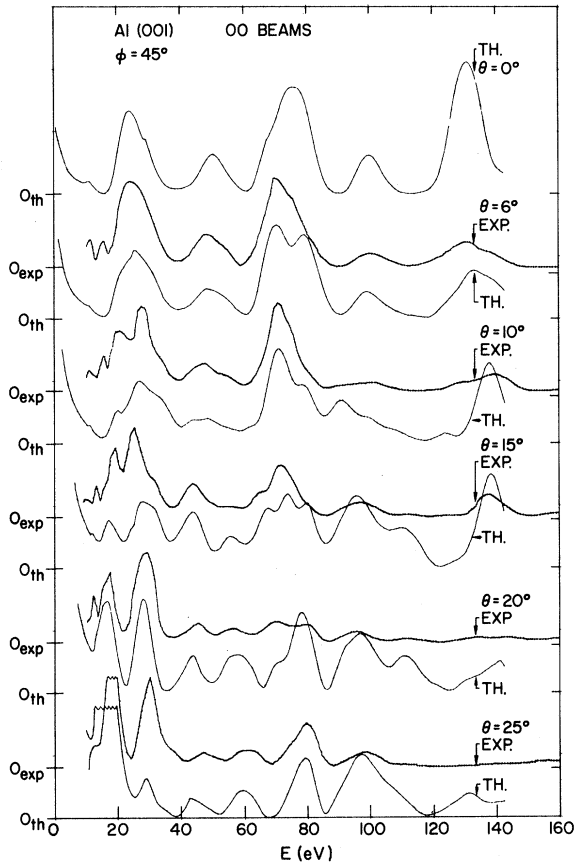


FIG. 3. Al{001}, 00 beam spectra, measured and calculated, as functions of polar angle $\theta$ at $\phi = 45°$. Calculated with Snow potential and absorption ($\beta = 4.1$ eV $= 0.30$ Ry), step of $-i\beta$ in potential at surface, spectra shifted $-7.5$ eV. Zero levels of experimental and theoretical curves marked for each angle.

(see Sec. IX). Our previous work concentrated on one angle, and it is desirable to test the validity of the model further by comparing theory and experiment for the extensive measurements on the angular variation of these spectra.[19] This comparison is made in Figs. 3, 4, and 5 for the 00 (specular), $1\bar{1}$ and $0\bar{2}$ beams, respectively, over the angular range $\theta = 6$–$25°$ at $\phi = 45°$. (See Fig. 2 for the conventions used on beam labels and the definition of $\phi$; the $\theta$ rotation of the crystal is assumed to occur horizontally in these figures, moving the 00 spot to the right for increasing $\theta$.)

The same general level of agreement between theory and experiment attained in our previous paper[1] at $\theta = 6°$, $\phi = 45°$ is reproduced here for the other angles although there are noteworthy differences at the higher angles. The positions of the experimental peaks generally correspond closely to theory; the relative amplitudes not so well, although there is reasonable correspondence. However, the correction for lattice motion has not been made in these calculations. There are no experimental data for the 00 beam at normal incidence, but we note from Fig. 3 that the theory predicts a fairly large peak (presumably a primary Bragg peak) at about 130 eV which drops in intensity by more than a factor of 2 when $\theta$ changes from 0 to 6°, and becomes asymmetric as a shoulder develops on the high-energy side. The experimental values should also be sensitive to angle, and proper comparison with theory requires that the experimental angles be very close to those of the theory.

The nonspecular beams (Figs. 4 and 5) exhibit, in general, large Bragg peaks which can be correlated with the Bragg reflections expected into these beams from the incident beam. Sizable "secondary" peaks,[20] such as those observed between the Bragg peaks in the 00 beam, are not observed here. As the $\theta$ angle is varied, most of the observed peaks persist, moving slowly to left or right as the angle changes, as expected from free-electron theory.[20] The peaks also show gradual changes in shape and intensity. Occasionally, some peaks seem to disappear or to change radically at certain angles. This fact has been observed and explained by several authors, quite properly we believe, in terms of scattering into Laue or into other Bragg beams that happen to satisfy the

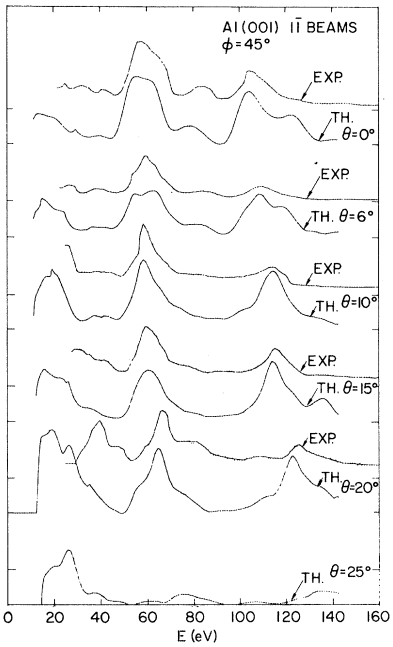


FIG. 4. Al{001}, $1\bar{1}$ beams, calculated as for Fig. 3. The experimental curves in Figs. 3 and 4 are slightly changed from the curves published in Ref. 19, where too large a correction was made for the dependence of incident current with energy. The change affects the nonspecular spectra and the relative peak heights, but not the specular spectra and the peak positions.

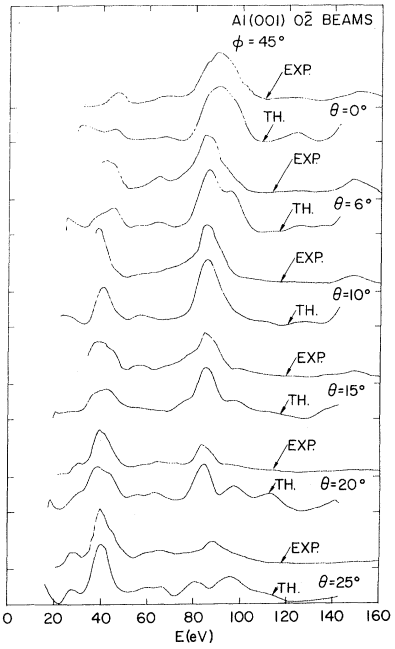


FIG. 5. Al{001}, 0$\bar{2}$ beams, calculated as for Fig. 3; experimental curves changed as for Fig. 4.

diffraction conditions simultaneously with the observed Bragg peak at the given energy and angle.[21,22] The theoretical curves presented here do not always seem to reproduce this effect at the angle observed experimentally. For example, Fig. 3 shows this effect at 20° in the experimental spectra in the peak around 70 eV whereas the theoretical spectra appear to show such a change nearer to 15°. Since the explanation in terms of other beams involves only bulk properties of the crystal, we conclude that this discrepancy might indicate that the potential used in the present calculations is not wholly adequate. Other discrepancies between theory and experiment may be due to surface effects which are not taken into account in the present model of an "ideal" surface. There is, in particular, some reason to believe that such effects have greater influence on the curves at angles far from normal incidence, as the electron path lengths in the surface region will be greater for electrons nearer to grazing incidence.

## V. CORRECTION FOR LATTICE MOTION

Lattice motion has a strong effect on LEED spectra, as can be seen from the experimentally observed temperature dependence of LEED intensities. The theory of the elastic and inelastic scattering given in Sec. II is plausibly and simply extended to a theory for a vibrating lattice by averaging the scattering of each atomic potential over the motion of that atom. This averaging gives an effective scattering by each atom at its mean position to which the theory for the rigid periodic lattice can be applied. This procedure is systematically developed from many-body perturbation theory by Duke and Laramore.[23,24] Note that averaging the scattering is not equivalent to averaging the potential and then finding the scattering; such a procedure would, for example, smear out the $(1/r)$ singularity of the potential at the nucleus and substantially reduce the scattering. It is inherent in the approximate treatment of lattice motion by average scattering that the atomic motions are treated as independent, and that correlations in the motions of neighboring atoms are neglected. Also a further approximation is made at this point for convenience of calculation, namely, that a Debye spectrum of lattice modes describes the motion of an atom adequately. A more realistic spectrum could be easily introduced, including a dependence of the motion on distance from the surface, if detailed information were available.

The scattering of an atom may be described by the matrix elements of its $t$ matrix[25] between plane-wave states. For a spherical atom these matrix elements can be expressed in terms of the phase shifts $\eta_l$ by the relation[26]

$$\langle \vec{k}' | t | \vec{k} \rangle = \sum_l t_l (2l+1) P_l(\cos\theta_{kk'}) , \tag{39}$$

$$t_l \equiv = -(e^{2i\eta_l} - 1)/2ik , \quad |\vec{k}'| = |\vec{k}| \tag{40}$$

where $P_l$ is the Legendre polynomial of order $l$, and $\theta_{kk'}$ the angle between $\vec{k}$ and $\vec{k}'$. Let $t_r$ be the $t$ matrix for an atom displaced by $\vec{r}$ from its normal position; then $t_r$ can be written in terms of the $t$ matrix at the original position by introducing the shifts in phase of the plane waves between the two positions[27]

$$\langle \vec{k}' | t_r | \vec{k} \rangle = e^{i(\vec{k}-\vec{k}')\cdot\vec{r}} \langle \vec{k}' | t | \vec{k} \rangle . \tag{41}$$

Averaging (41) over lattice motions gives

$$\langle \langle \vec{k}' | t_r | \vec{k} \rangle \rangle_{\mathrm{Av}} = \langle e^{i(\vec{k}-\vec{k}')\cdot\vec{r}} \rangle_{\mathrm{Av}} \langle \vec{k}' | t | \vec{k} \rangle , \tag{42}$$

where the first factor in the right, the Debye-Waller factor, when $\vec{r}$ is averaged over a Debye spectrum of lattice modes, is[28]

$$\langle e^{i(\vec{k}-\vec{k}')\cdot\vec{r}} \rangle_{D\ \mathrm{Av}} = e^{-A(\vec{k}-\vec{k}')^2} , \tag{43}$$

$$A \equiv \frac{3\hbar^2}{2Mk_B\Theta_D} \left[ \frac{1}{4} + \left( \frac{T}{\Theta_D} \right)^2 \int_0^{\Theta_D/T} \frac{x\,dx}{e^x - 1} \right] , \tag{44}$$

where $M$ is the mass of an atom, $k_B$ is the Boltzmann constant, and $\Theta_D$ is the Debye temperature. Using the standard formula[29]

$$e^{i\vec{k}\cdot\vec{r}} = \sum_l (2l+1) i^l j_l(kr) P_l(\cos\theta_{kr}) ,$$

$$l = 0, 1, \ldots, \infty \tag{45}$$

(43) becomes

$$\langle e^{i(\vec{k}-\vec{k}')\cdot\vec{r}}\rangle_{D\ Av} = e^{-2Ak^2}\sum_l (2l+1) i^l j_l(-2iAk^2) \times P_l(\cos\theta_{kk'}) . \quad (46)$$

Putting (39) and (46) into (42) gives

$$\langle\langle \vec{k}' | t_r | \vec{k}\rangle\rangle_{D\ Av} = e^{-2Ak^2} \sum_{l_1 l_2} t_{l_1} i^{l_2} j_{l_2}(-2iAk^2)(2l_1+1)(2l_2+1) \times P_{l_1}(\cos\theta_{kk'}) P_{l_2}(\cos\theta_{kk'}) . \quad (47)$$

Using a standard formula in the theory of angular momentum[30]

$$P_{l_1}(\cos\theta) P_{l_2}(\cos\theta) = \sum_l \begin{pmatrix} l_1 & l_2 & l \\ 0 & 0 & 0 \end{pmatrix}^2 (2l+1) P_l(\cos\theta), \quad (48)$$

where $\begin{pmatrix} l_1 l_2 l \\ 0 0 0 \end{pmatrix}$ is the Wigner 3-$j$ coefficient, in (47) gives

$$\langle\langle \vec{k}' | t_r | \vec{k}\rangle\rangle_{D\ Av} = \sum_l \tau_l (2l+1) P_l(\cos\theta_{kk'}), \quad (49)$$

with

$$\tau_l \equiv e^{-2Ak^2} \sum_{l_1 l_2} t_{l_1} \begin{pmatrix} l_1 & l_2 & l \\ 0 & 0 & 0 \end{pmatrix}^2 (2l_1+1) \times (2l_2+1) i^{l_2} j_{l_2}(-2iAk^2) . \quad (50)$$

Comparing (49) to (39) shows that $\tau_l$ in the Debye-averaged matrix element corresponds precisely to $t_l$ in the matrix element at the original position. Hence, effective (complex) phase shifts $\overline{\eta}_l$ for the scattering averaged over the motion could be defined by

$$\tau_l \equiv -[e^{2i\overline{\eta}_l} - 1]/2ik \quad (51)$$

and used in the LEED theory of Sec. II. In fact, the LEED theory uses the particular function of phase shifts given in (51) or (40), as shown by (29).

The changes that occur in the calculated LEED spectra when this correction for lattice motion is added to the effects of absorption are shown in Fig. 6, which gives the results for Al{001} at $\theta = 6°$, $\phi = 45°$, $\Theta_D' = 418\,°K$, and the same potential, matching condition and energy shift as used in Sec. IV. The results of a similar calculation at normal incidence with and without absorption are shown in Ref. 1. (Real values of $k^2$ were used in the calculation of $\tau_l$, consistent with our use of real phase shifts for an atom imbedded in an inelastically scattering medium.) The correction for lattice motion introduces a new mechanism of incoherent scattering which, like the absorption, broadens and reduces the peaks, and acts similarly to an energy-dependent imaginary part to the potential inside the atomic-scattering potentials. The overall effect is similar to that of a Debye-Waller factor in x-ray diffraction theory; i.e., the intensities at higher energies are reduced much more than those at lower energies. Figure 6 shows the effect is to give a substantial improvement in the agreement between theory and experiment, e.g., the double peak in the 00 beam at 77 eV is converted to a single peak, and a similar change occurs in the $0\bar{2}$ beam at 90 eV. The relative intensities are now closer to experiment, although the theoretical peak at 26 eV in the 00 beam is too high and the $1\bar{1}$ peak at 60 eV does not have the right shape—other differences between theory and experiment lie within the error of the measurements.[31]

## VI. EFFECTS OF DIFFERENT METHODS OF MATCHING WAVES AT THE SURFACE

Our first matching method is based on the simplest assumption about matching fields across the surface of the crystal in a LEED calculation; namely, we truncate the potential of an infinite crystal halfway between two planes of atoms and put the constant vacuum level on one side. Then continuity of the wave field and its normal derivative at this abrupt step in both the real and imagin-

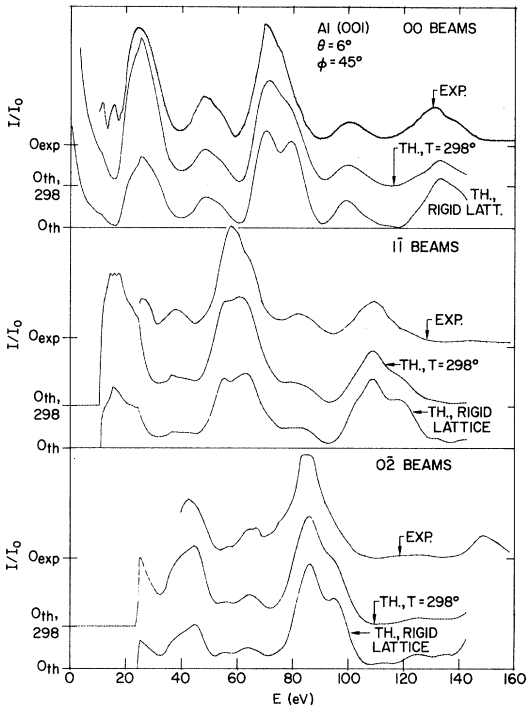


FIG. 6. Effect of temperature corrections on Al{001} spectra for $\theta = 6°$, $\phi = 45°$; potential and surface matchings as for Fig. 3; spectra at $T = 298\,°K$ computed with Debye spectrum of lattice motions at $\Theta_D = 426\,°K$, compared with rigid lattice and experimental spectra. Values on the ordinate scales for peak energy, $I/I_0$ (rigid lattice), and $I/I_0$ ($T = 298\,°K$) correspond, respectively, to the following: for the 00 beam, 70.5, 0.053, and 0.019; $1\bar{1}$ beam, 62.5, 0.020, and 0.0092; $0\bar{2}$ beam, 86.5, 0.028, and 0.0085.

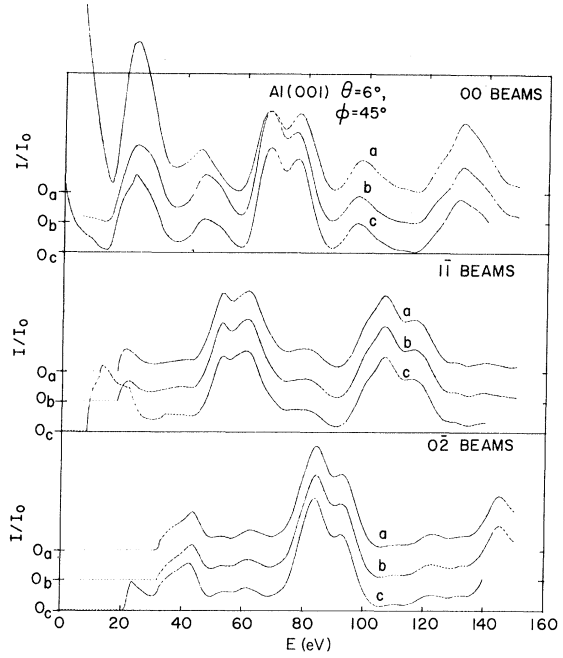


FIG. 7. Effects of different matching procedures on calculated Al{001} spectra at $\theta = 6°$, $\phi = 45°$, $\beta = 4.1$ eV for 00, $1\bar{1}$, and $0\bar{2}$ beams. Plots a: abrupt step at surface in real and imaginary part of potential $-7.5 - 4.1i$ eV. Plots b: no-reflection matching (see Sec. VI). Plots c: $\beta$-reflection matching (abrupt step only in imaginary part of potential, spectrum calculated and shifted $-7.5$ eV).

ary parts of $V(\vec{r})$ and consideration of the boundary condition at infinity determine a unique LEED problem. The result of this procedure applied to Al{001} generates the LEED curve marked (a) in Fig. 7. This method of matching has the drawback that the artificial abrupt step in the potential produces an unphysically large reflection. The actual potential has a gradual change from vacuum to crystal interior[32] which would produce a much smaller reflection.

A second matching method is based on the simplest way to eliminate these artificially strong reflections; namely, we calculate the LEED spectra produced by a potential without the abrupt step by moving the muffin-tin zero (the real part of $V_0$) up to the vacuum level. At normal incidence a consequence of this procedure is to translate both the band structure of the crystal and the peaks in the LEED spectra toward higher energies by the same amount. Thus the calculated spectra must be translated back by this amount to put the peaks at their correct energies.[33] This translation was determined empirically to be 7.5 eV for Al{001} by shifting the calculated spectra to get the best match with experiment (at $\theta = 6°$). The discrepancy between this value and the shift value of 12.4 eV expected from the experimental work function will be discussed in Sec. IX. This procedure with a shift of 7.5 eV was used to calculate all the curves in Figs. 3, 4, 5, 6 and curves (c) in Fig. 7.

This second matching method, however, has two failings: (i) By eliminating the potential step we also eliminate the change in angle that occurs when the beams are refracted through the surface. Refraction, which is governed by Snell's law, is independent of how the potential varies through the surface and therefore occurs even when the potential varies gradually. Thus, the fact that we have eliminated the abrupt potential step is equivalent to saying that the incidence angles quoted in the figures are the angles made with the surface normal by the primary beam inside the crystal rather than by the primary beam in vacuum as they should be. The differences between these angles vanish, of course, at normal incidence, and are believed to be smaller than the experimental error in all other curves shown here. (ii) The method does not eliminate the small amount of reflection at the surface that is caused by the sharp step in the imaginary part of the potential (from zero in vacuum to the value $-0.3$ Ry) used in our calculations on Al{001}). Although the effect of this step appears to be small, note, however, the pointed shape of the leftmost peak in the 00 spectrum of (c) that does not occur in the other spectra in Fig. 7. For the purposes of the present discussion we call this matching method the "$\beta$-reflection" method ($-i\beta$ being the imaginary part of the potential $V_0$).

In the third matching method to be considered, it is assumed that the incident beam from vacuum arrives on the crystal side of a gradual potential step of unspecified profile without having suffered any reflection in the step region. The beam has the same intensity and $k_p$ value as outside the crystal, but a new $k_z$ value given by $k_z = (E - V_0 - k_p^2)^{1/2}$ as it moves between scatterers inside the crystal. Similarly, it is assumed that all beams incident on the step from inside the crystal join on to the corresponding waves in vacuum without any reflection back into the crystal. For short, call this the "no-reflection" matching procedure.[34]

At normal incidence, the intensity of reflection at any energy above the muffin-tin zero is independent of the step height, so that any value of the real part of $V_0$ may be used in the calculation and the best value of this quantity determined by shifting the spectra to match experiment. Calculations away from normal incidence can then be carried out with the best value of the real part of $V_0$ so that the refraction of the incident beam is taken into account properly. (Note that the spectra for oblique incidence would not translate rigidly with change of $V_0$.) The no-reflection procedure applied to Al{001} gives the curves (b) in Fig. 8. All

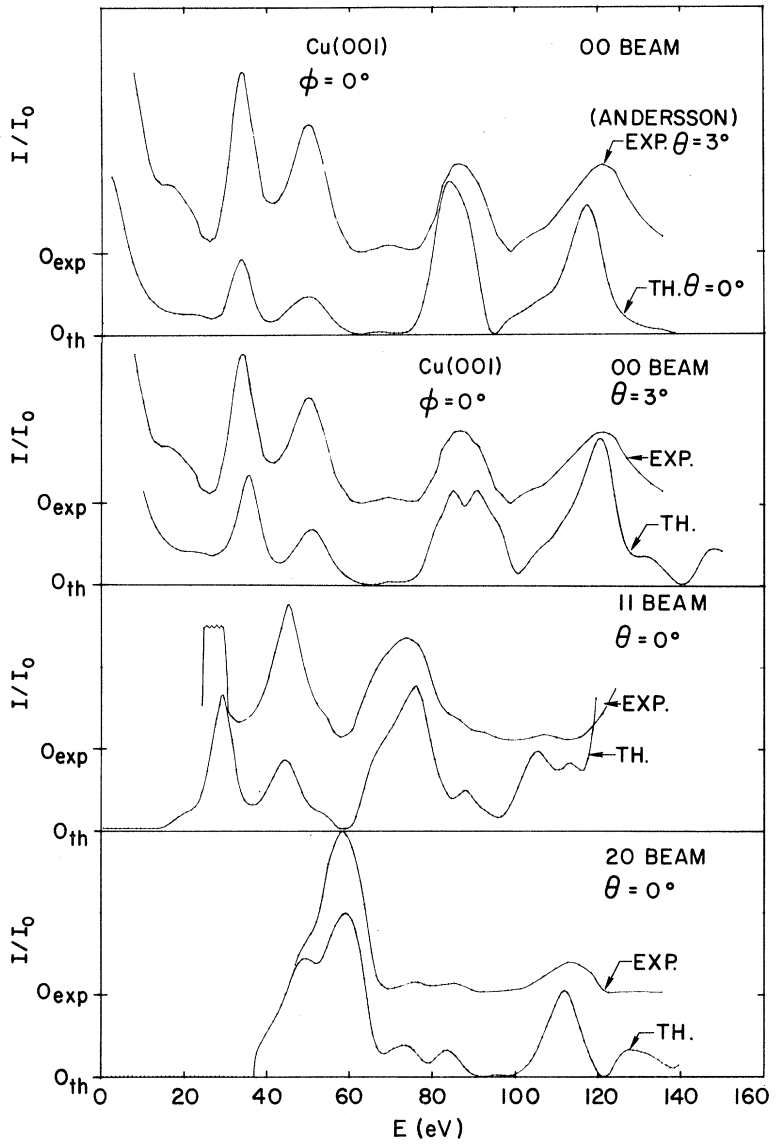


FIG. 8. Cu{001} spectra at and near normal incidences for $\phi = 0°$, comparing theory and experiment. Theory uses Chodorow potential (Ref. 36), with imaginary part $\beta = 3.4$ eV (0.25 Ry), rigid lattice, no reflection matching, and a shift of $-9.5$ eV. In plot 1 (top) theory and experiment are for different $\theta$'s, showing differences.

calculations on Cu and Ag in this paper used this procedure.

A possible defect of both the "$\beta$-reflection" and the "no-reflection" methods is that those beams in the crystal which move toward the surface in directions such as to be totally internally reflected are not reflected at all in the "no-reflection" method and only slightly in the $\beta$-reflection method. Instead, these beams are assumed to match decaying vacuum waves without reflection. This assumption is a good one if such beams are in fact strongly inelastically scattered by surface excitations such as surface plasmons. To test the consequences of this assumption in the present case, which has no special surface scattering, we have carried out calculations in which proper total internal reflections were imposed for those beams, but no reflections at all were assumed for the beams that physically pass through the surface. The results were essentially the same as curves (b).

The curves in Fig. 7 show some differences in the shapes of the lowest peaks of the 00 and $1\bar{1}$ beams, but generally the different matching methods do not affect the spectra much, particularly the nonspecular beams and the higher-energy parts of the 00 spectra. A tentative conclusion is that the spectra above about 40 eV are insensitive to the actual shape of the electronic potential profile between vacuum and the crystal interior. These high-energy parts of the spectra may thus be more suitable for obtaining the structure of the surface layers, i.e., the atomic positions, than the low-energy parts.

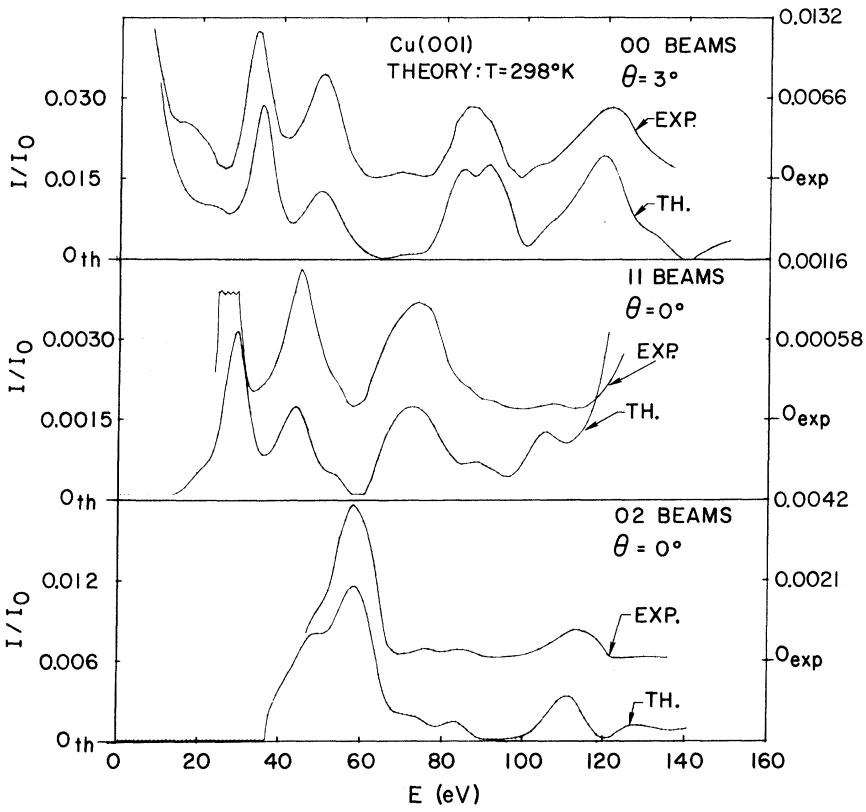


FIG. 9. Cu{001} spectra as in Fig. 8 but containing the lattice motion correction with $T=298\,^{\circ}\mathrm{K}$, $\Theta_D=339\,^{\circ}\mathrm{K}$.

## VII. COMPARISON OF THEORY AND EXPERIMENT FOR Cu{001}

Figures 8 and 9 show comparisons between the experimental data of Andersson[35] for the {001} face of copper and calculations made with the potential of Chodorow as quoted by Burdick[36] with the addition of an imaginary part $-i\beta$, $\beta = 0.25$ Ry. As for Al{001} the calculations reproduce both the primary and the secondary structure of the spectra fairly well. Note that the calculated spectrum is a sensitive function of the angle of incidence: Fig. 8, plot 1 compares the 00 spectrum calculated for normal incidence with that measured at an angle of incidence 3° away from normal. There is definite disagreement between the two spectra, which disappears when the calculation is repeated for the actual experimental angle of incidence (plot 2). These two cases emphasize the fact that it can be important to carry out the calculations at the same angle for which the experiment was done. In Fig. 8, plots 2, 3, 4, the experimental 00, 11, and 20 spectra are compared with the results of calculations done for the rigid lattice, and Fig. 9 does the same for calculations valid at 298 °K, i.e., including the correction for lattice motion with $\Theta_D = 339\,^{\circ}\mathrm{K}$ discussed in Sec. V. We note again that consideration of the lattice motion improves the agreement between theory and experiment. Andersson gives the magnitudes of the reflected flux as a fraction of the incoming flux. The calculated spectra are generally a factor of 2 to 3 greater than his measured values, as can be seen by comparing the scales on the two sides of Fig. 9. Such a difference is not surprising because one would expect that only a fraction of the surface is regular enough to contribute to LEED. Without the lattice-motion correction the calculated intensities are of the order of ten times the experimental measurements.

Calculations have been made previously for Cu{001} by Capart,[37] who also compared his results with Andersson's data. Our results appear to correspond more closely to the experiment than Capart's. We note three differences in the method of calculation: Capart performed his calculations only for normal incidence, which immediately reduces the degree of correspondence that can be hoped for; he used only three phase shifts in his calculations, against eight used in ours; he used the KKRZ method, which effectively eliminates the $\vec{r}$ space sums of the Ewald procedure (which we include) thus reducing the accuracy which can be expected *a priori*.

Both our calculations and Capart's make use of phase shifts as the atomic-scattering input for the

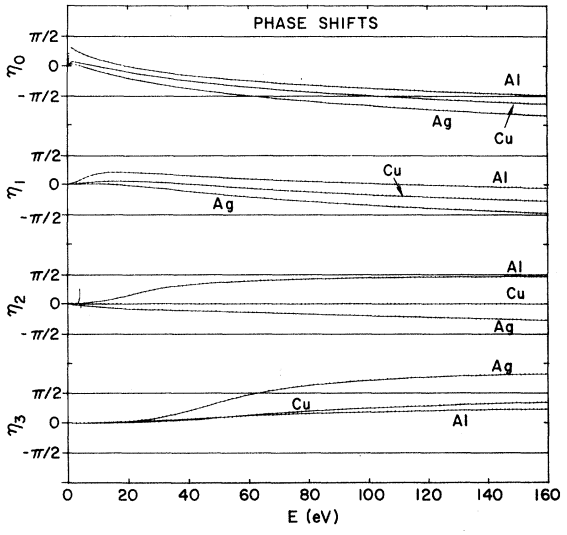


FIG. 10. Energy dependence from 0 to 160 eV of the phase shifts $\eta_l(E)$ for $l=0$, 1, 2, 3 used in the Al, Cu, and Ag calculations, where $\eta_l(0)=0$. Note that $\eta_2$ for Cu at 4.5 eV shows a rapid increase of $\pi$ in magnitude, which is subtracted from the higher-energy part of the curve. The energies are measured with respect to the muffin-tin zero, not with respect to vacuum, since the curves describe properties of the isolated atomic sphere.

LEED intensity calculations; this permits direct comparison of the atomic scattering. The phase shifts we used are depicted in Figs. 10 and 11. The most striking difference between these curves and those given by Capart is that our $s$ phase shift goes through $\frac{1}{2}\pi$ at approximately 100 eV while Capart's passes through this scattering maximum at only 60 eV. It is not clear whether this difference in the phase shifts accounts for the difference in the LEED spectra or whether the difference in calculational procedures is important.[38]

## VIII. LEED SPECTRA FOR Ag{001} AND COMPARISON WITH Cu{001} AND Al{001}

Silver is another fcc material for which a self-consistent band-structure potential is available.[39] The phase shifts computed from this potential are markedly different from those of aluminum and copper, as we can see from Figs. 10 and 11. The differences are revealed more directly by the partial-wave contributions $\sigma_l$ to the total scattering cross section $\sigma$ of a single metal atom than by the phase shifts, and are given by the formulas

$$\sigma=\sum_l \sigma_l \tag{52}$$

and

$$\sigma_l=\frac{2l+1}{4\pi k^2}\sin^2\eta_l\,, \tag{53}$$

where $\eta_l$ is the $l$th phase shift. Note that the definition of $\sigma_l$ includes the factor $(2l+1)$, the number of spherical waves with this phase shift, a factor that weights the higher phase shifts more than the lower ones. The expression for $\sigma_l$ is largest when $\eta_l$ goes through $(n+\frac{1}{2})\pi$. A relatively small change in the potential can displace the phase-shift curve enough to move the maximum of $\sigma_l$ to quite a different energy range.

The energy dependences of the $\sigma_l$'s for aluminum, copper, and silver are given in Fig. 12 in units of $a_0^2$ (the Bohr radius squared) and can be compared with the cross sectional area of the unit mesh of atoms in a plane parallel to the surface of the crystal. For silver and aluminum this mesh area is nearly the same ($29.8a_0^2$ and $29.3a_0^2$, respectively),

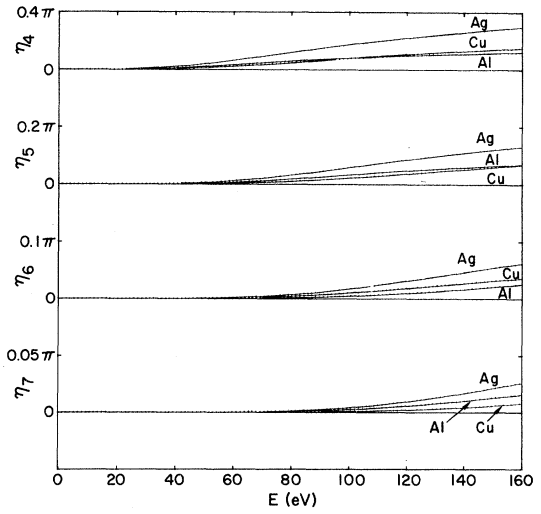


FIG. 11. $\eta_l(E)$ as in Fig. 10 for $l=4$, 5, 6, 7.

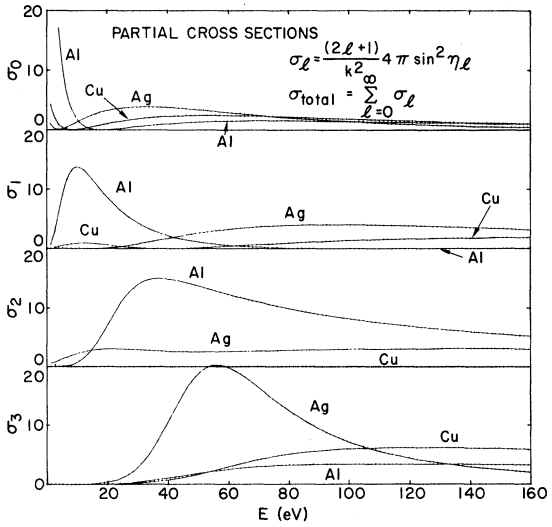


FIG. 12. Energy dependence from 0 to 160 eV of the partial cross sections $\sigma_l(E)$ for $l=0$, 1, 2, 3.

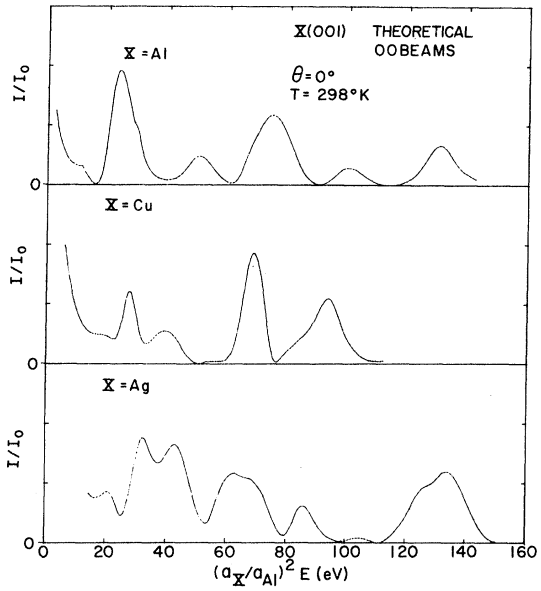


FIG. 13. Comparative plots of 00 beam {001} spectra at normal incidence of the previously described calculations for Al and Cu with a calculation for Ag as in Fig. 16, on a reduced energy scale (Ref. 40); $(a_{Cu}/a_{Al})^2 = 0.80$, $(a_{Ag}/a_{Al})^2 = 1.18$. Calculations include lattice-motion corrections at $T = 298\,°K$.

while for copper it is somewhat smaller ($23.3a_0^2$). We note that at approximately 55 eV the $f$ wave alone, i.e., $\sigma_3$, for silver makes a contribution of $\frac{2}{3}$ of the mesh area and that the sum of the contributions of all phase shifts exceeds the mesh area. The partial cross sections of copper and aluminum as calculated here are generally smaller; hence, we expect to find the LEED spectrum of silver less free-electron-like than that of either aluminum or copper. This expectation seems to be borne out by the calculations of the LEED spectra of the specular beams from the {001} surfaces as shown in Fig. 13. This figure compares the theoretical spectra at normal incidence for Al{001}, Cu{001}, and Ag{001} on a reduced energy scale,[40] and shows that the phase shifts of the three metals are sufficiently different to predict quite different LEED spectra. (The Debye temperature used in all silver calculations was 225 °K and $\beta$ was 0.25 Ry). Since the experimental data for the specular beams at normal incidence are not available, these curves cannot be compared with experiment. However, Fig. 14 and Fig. 15 compare the nonspecular beams 11 and 20 at normal incidence for Al, Cu, and Ag{001} with one another and show that the experimental data confirm the differences predicted and are reproduced quite well by the theory.

In Figs. 14 and 15, the experimental data for Al{001} are those of Jona[19] and for Cu{001} those of Andersson.[35] The Ag{001} data were taken on single-crystal silver film grown epitaxially on a rock-salt substrate[41]—they should be considered preliminary because of experimental difficulties, including the possibility of surface contamination by chlorine originating from the film substrate. Data on the Ag{001} at an angle of incidence of 10° are compared to the corresponding theoretical spectra in Figs. 16 and 18 and the nonspecular beams for $\theta = 0°$ in Fig. 17. Below approximately 40 eV in the 00 beam (Fig. 16) there is practically

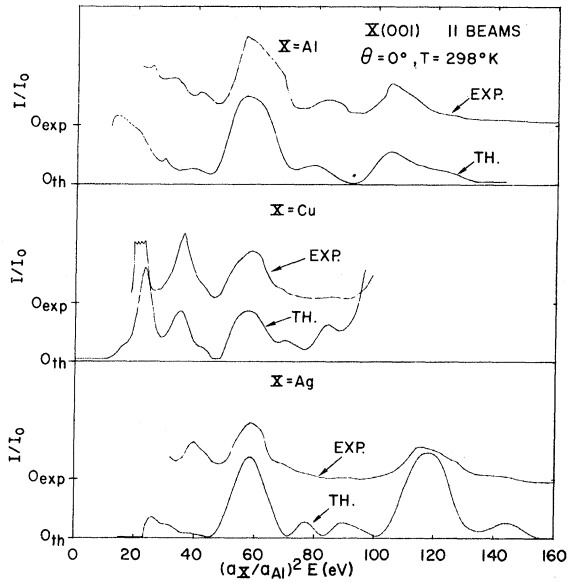


FIG. 14. Comparative plots of 11 beams, as in Fig. 13.

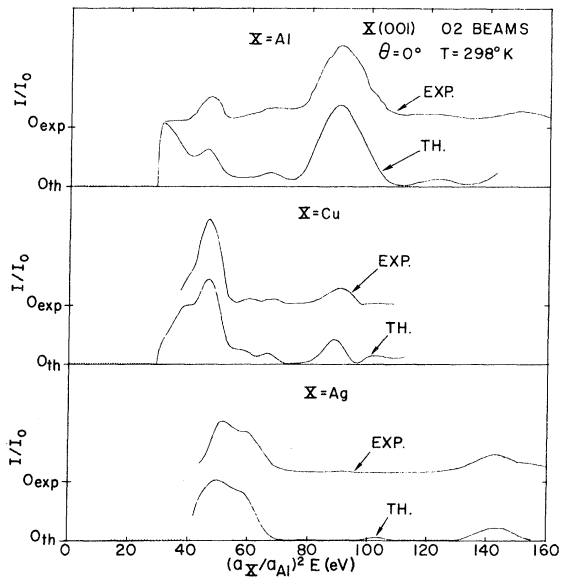


FIG. 15. Comparative plots of 20 beams, as in Fig. 13.

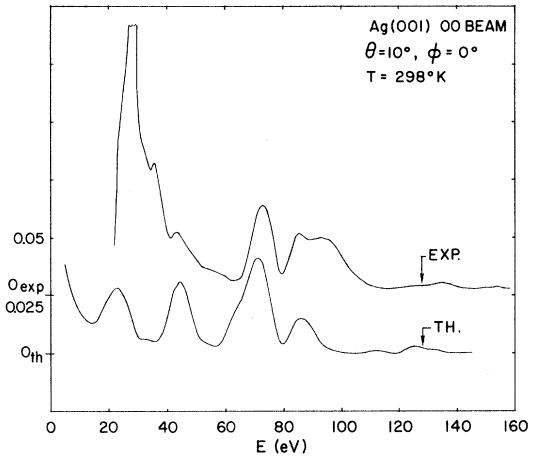


FIG. 16. Ag{001}, 00 beam spectra measured and calculated, at $\theta = 10°$, $\phi = 0°$. Calculations use Snow potential (Ref. 39) and absorption with $\beta = 3.4$ eV, no reflection matching with step of $-5.0$ eV, correction for lattice motion at $T = 298\,°K$ with $\Theta_D = 225\,°K$.

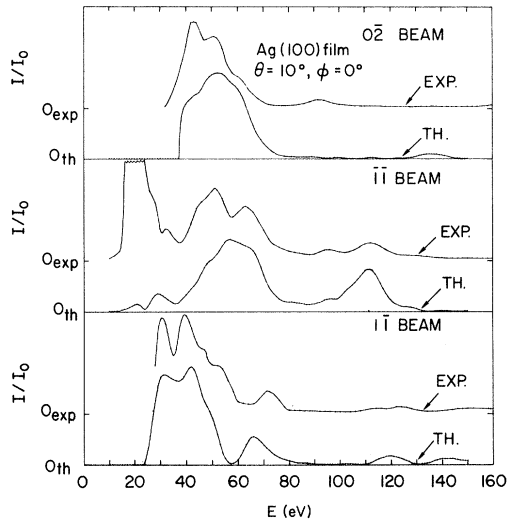


FIG. 18. Ag{001}, spectra for $\theta = 10°$, $\phi = 0°$, 0$\bar{2}$, $\bar{1}\bar{1}$ and 1$\bar{1}$ beams; calculations as in Fig. 16. These spectra, with Fig. 16, give all beams in the first three shells at the given angles.

no correspondence, which may be due either to inaccuracies of the potential or to the presence of surface impurities or other experimental difficulties. Note that the $\bar{1}\,\bar{1}$ and $1\,\bar{1}$ beams at $\theta = 10°$ (Fig. 18) differ much more from each other than from the calculated spectra, and also from the $1\,\bar{1}$ beams at $\theta = 0°$ (Fig. 17).

In conclusion, we point out again that the Snow band-structure potential for silver predicts surprisingly large partial cross sections for the silver atom at LEED energies. It is in fact found that

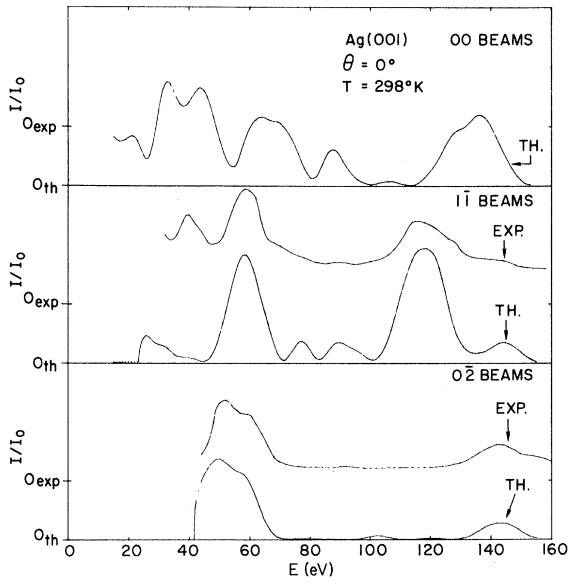


FIG. 17. Ag{001}, spectra at normal incidence, 00, 1$\bar{1}$ and 0$\bar{2}$ beams, calculations as in Fig. 16.

the LEED spectra of Ag{001} are both stronger and more sensitive to the angle of incidence than the corresponding spectra for aluminum, which may well be a consequence of the greater scattering power of the silver atom.

## IX. LEED SPECTRA AND ENERGY DEPENDENCE OF THE EXCHANGE-CORRELATION POTENTIAL

In Sec. VI, we have described how LEED calculations can be performed at normal incidence without fixing the quantity $\Delta$, which measures the real part of the potential between the atoms in the crystal relative to vacuum, and how $\Delta$ can then be empirically evaluated by shifting a calculated spectrum to match the corresponding measured spectrum; a single $\Delta$ for each metal could then be used to give satisfactory agreement for all beams at all angles of incidence. We now discuss the expected value of $\Delta$ arising from a simple static model of the crystal potential and the reasons why this expected value and the empirical value differ.

The simple static model of the crystal potential uses a band-structure potential (e.g., the Snow potential for Al) which is supplemented by a constant imaginary part and fixed relative to vacuum by the measured work function. The static potential model would then determine the one-electron energy levels of the scattering system and hence the value of $\Delta$. For example, we note the following energy levels (the numerical values are for Al using the Snow potential): the vacuum level—outside the {001} surfaces (for convenience fix its value at

0); the Fermi level, which lies below the vacuum level by the work function (−4.2 eV); the average potential between atoms or muffin-tin zero (8.2 eV below the Fermi level, hence −12.4 eV); the bottom of the conduction band (−15.2 eV); and the volume average potential (−20.4 eV). Thus the expected $\Delta$ for Al is −12.4 eV to be compared to the empirical value of −7.5 eV.[42] We believe the explanation of this difference is that the above potential model and energy levels apply to a slowly moving electron, whereas the empirical value refers to an electron at LEED energies up to 150 eV. To bring out the difference between potentials for slow and fast electrons, note that the one-electron potential may be regarded as a combination of two parts[44]: (i) an electrostatic potential due to the charge distribution of the crystal, including both the periodic charge and the charge in the surface region tailing off into vacuum and giving rise to a dipole layer; (ii) an exchange-correlation potential $V_{xc}$ which corrects for the detailed interaction of the electrons, taking account of the exchange and correlation "holes" in the distribution around a given electron. The first part is independent of the energy of the electron, but the second part is really energy dependent and if this dependence is taken into account, the energy levels above will be modified.

A detailed theory of $V_{xc}$ in a crystal is not now available, but we can obtain some idea of its magnitude and behavior from the theory of the uniform electron gas[13] of the same average electron density, i.e., the same density as the conduction electrons, a density corresponding to $r_s = 2.07a_0$ for Al. This theory identifies $V_{xc}$ with part of the electron self-energy and yields the imaginary part $-i\beta$ of $V_{xc}$ used in the LEED spectra calculations (an average $\beta$ of 4.1 eV was used for Al). The real part of $V_{xc}$ rises by 5.5 eV between the vacuum level (15.8 eV above the bottom of the band, since the Fermi energy of the free-electron gas is 11.6 eV) and 100 eV above the vacuum level, and is quite flat above 100 eV. Thus we can expect that fitting the calculated spectrum to the measured spectrum around and above 100 eV would require a shift $\Delta$ of $-12.4 + 5.5 = -6.9$ eV, in surprisingly good agreement with the value −7.5 eV previously found for $\Delta$. With this $\Delta$, calculated peaks at lower energies should be slightly too high, as appears to be the case, for example, for the peak around 25 eV in the 00 spectrum of Al{001} in Fig. 6. However, the total magnitude of the change in $V_{xc}$ (5.5 eV), although observable, is still small compared to the range of 100 eV. Hence, the simple static model of the crystal potential works fairly well. There is some indication that the changes with energy of the exchange and correlation considered separately would be substantially larger. Overhauser[45] estimates the exchange and correlation energies separately as functions of energy in a uniform electron gas, although only over a small range of energies above the Fermi level, and shows a near cancellation of the sum of the changes. This near cancellation, although derived only for the uniform gas, suggests that it is not adequate to introduce only the energy dependence of exchange, at least for the valence electrons.

The magnitude of the real part of the exchange-correlation potential in a real crystal should become smaller at high energies like in the uniform electron gas, since this change results from the decreased correlation between the incoming electron and the electrons of the crystal when the incoming electron has a high velocity. An equivalent statment is that the self-energy, work function, and image potential all become smaller as the electron energy increases. Because the results with an energy-independent potential match up the peaks in the spectrum over the whole range from 30 to 150 eV particularly well, it is further suggested that the exchange-correlation contributions in the real crystal vary less with energy in this range than do the contributions for the uniform electron gas. However, the value of the exchange-correlation between 30 and 150 eV, although nearly constant, is different from the low-energy value which enters into the calculation of the work function.

For Cu{001} an experimental value of $\Delta = -9.5$ eV is determined by shifting the calculated spectra to match the measurements; similarly for Ag{001} the experimental value is $\Delta = -5.0$ eV. The potential used for Cu gives the Fermi level 7.7 eV above the muffin-tin zero[36,43]; for Ag the corresponding figure is 6.4 eV.[39,43] The static work function[46] for Cu is 4.5 eV and for Ag, 4.4 eV. Thus the expected level change between vacuum and the muffin-tin zero is −12.2 eV for Cu and −10.8 eV for Ag. We correct these in the same way as for Al, by using the change in the real part of $V_{xc}$ taken from Lundqvist's curves[13] for the real part of the self-energy of the uniform electron gas at an $r_s = 2.67a_0$ for Cu and $r_s = 3.02a_0$ for Ag. Thus for Cu the rise in $V_{xc}$ between the vacuum level (which is 11.5 eV above the bottom of the conduction band since the Fermi energy is 7.0 eV) and an energy 100 eV above the vacuum level is 5.0 eV; similarly for Ag (Fermi energy 5.5 eV) the change in $V_{xc}$ between vacuum level and 100 eV above is 5.2 eV. Hence the corrected calculated values of $\Delta$ are $-12.2 + 5.0 = -7.2$ eV for Cu and $-10.8 + 5.2 = -5.6$ eV for Ag to be compared with experimental values −9.5 and −5.0, respectively. The value for Cu is not as close as for Al and Ag, but all three values are reasonably close,[47] and show the same qualitative result that the work function contribution to $\Delta$ is smaller in magnitude at higher ener-

gies.

In summary, if this explanation of the shift is correct, then comparison between LEED theory and experiment offers a prospect of obtaining information on the energy dependence of exchange-correlation energies in real crystals, and of evaluating theories of this quantity. In view of the large number of assumptions required to handle exchange and correlation in calculations for real crystals, such information would be very useful.


## ACKNOWLEDGMENTS

The authors are greatly indebted to A. R. Williams both for contributions of important parts of the programs used in the calculations and for valuable discussions of the formulation and application of the layer-KKR method. We are also indebted to S. Y. Tong for an illuminating discussion of the energy dependence of the real part of the self-energy and its significance for the level change $\Delta$.


---

*Work sponsored in part by the U. S. Air Force Office of Scientific Research of the Office of Aerospace Research.


[1]D. W. Jepsen, P. M. Marcus, and F. Jona, Phys. Rev. Letters 26, 1365 (1971).

[2]V. Hoffstein and D. S. Boudreaux, Phys. Rev. Letters 25, 512 (1970).

[3]C. B. Duke and C. B. Tucker, Jr., Phys. Rev. Letters 23, 1163 (1969).

[4]C. B. Duke, A. J. Howsmon, and G. E. Laramore, J. Vac. Sci. Technol. 8, 10 (1971).

[5]S. Y. Tong and T. M. Rhodin, Phys. Rev. Letters 26, 711 (1971).

[6]A preliminary account of the work of this paper was given at the Fifth LEED Seminar, Natl. Bur. Std., Washington, D. C., March 18 and 19, 1971.

[7]D. W. Jepsen and P. M. Marcus, *Computational Methods in Band Theory* (Plenum, New York, 1971), p. 416.

[8]P. M. Marcus and D. W. Jepsen, Phys. Rev. Letters 20, 925 (1968).

[9]J. Korringa, Physica 13, 392 (1947).

[10]K. Kambe, Z. Naturforsch. 22a, 322 (1967); 22a, 422 (1967); 23a, 1280 (1968); *Computational Methods in Band Theory* (Plenum, New York, 1971), p. 409.

[11]P. J. Jennings and E. G. McRae, Surface Sci. 23, 363 (1970).

[12]E. C. Snow, Phys. Rev. 158, 683 (1967).

[13]B. I. Lundqvist, Phys. Status Solidi 32, 273 (1969).

[14]The beam representation is an old and natural one for surface problems that has been used by many workers, e.g., M. von Laue, Phys. Rev. 37, 53 (1931); K. Hirabayashi and Y. Takeishi, Surface Sci. 2, 566 (1964). The idea is implicit in the work of C. G. Darwin, Phil. Mag. 27, 675 (1914), who discussed multiple scattering between layers using two beams, which was generalized to $N$ beams by E. G. McRae, Surface Sci. 11, 479 (1968). The same representation is used in an approach by N. Marcuvitz to the band problem, which arose from analogies with waveguide theory [Memorandum No. 9, Electrophysics Group, Polytechnic Institute of Brooklyn, 1956 (unpublished)]. Marcuvitz develops a similar transfer-matrix formalism, and derives, for example, the expansion of the Green's function in the beam representation given in (34).

[15]J. W. D. Connolly, Intern J. Quantum Chem. 3 S, 807 (1970).

[16]A few discrepancies appeared in limited regions when plot 4 of Fig. 1 and Connolly's published plot (Ref. 14) were superposed. In correspondence with Professor Connolly, he noted that in general his curves are interpolated from widely spaced points along $\Gamma X$, and a slight revision of the interpolated parts would give curves with no essential difference from ours. In addition, between 4.0 and 4.5 Ry, he found two levels that had been overlooked in the original APW calculation, and with addition of these levels a number of band shapes were altered so as to agree closely with ours.

[17]A. R. Williams (private communication).

[18]In recent papers by G. E. Laramore, C. B. Duke, A. Bagchi, and A. B. Kunz, Phys. Rev. B 4, 2085 (1971), and by G. E. Laramore and C. B. Duke, *ibid.* 5, 267 (1972), on the LEED spectra of Al {001} (and other faces) calculated by the inelastic-collision model, these authors find reasonable agreement with experiment near normal incidence but not very good agreement at larger angles of incidence on the {001} faces (and serious discrepancies for other faces). The results presented here give better agreement on {001} at all angles in terms of positions and shapes of peaks (and also for other faces, as will be discussed in a subsequent paper). We wish to point out an important difference between the work of these authors and ours, aside from the difference in method of calculation, which may well account for our different results. Although these authors also obtain their potential from the work of Snow (Ref. 12), we believe they have misinterpreted the potential constructed by Snow, since they take the value between spheres (the muffin-tin zero $V_0$) as $-1.225$ Ry but the value at the muffin-tin radius $RI$ as $-0.883$ Ry as given in Snow's Table I. These assumptions introduce a discontinuity of $-0.342$ Ry at $RI$ (for increasing $r$) which has an important effect on the phase shifts and on the band structure. In contrast, we use the potential in Snow's Table I, but with a small discontinuity of $+0.052$ Ry at $RI$ to $V_0 = -0.831$ Ry (the value given in the caption of Table I), which is consistent with the usual interpretation of $V_0$ for muffin-tin potentials as the average value over the space between spheres—hence slightly greater than the atomic potential at $RI$. Our interpretation is confirmed by the agreement between our band structure and those of both Snow and Connolly (e.g., from Snow's Table I, energies at $\Gamma$ and $X$ for the conduction band are $-0.207$, 0.390 Ry for $V_0 = 0$ while Connolly's corresponding values are $-0.202$, 0.389 Ry and our value at $X$ is 0.388 Ry). Thus if one uses Snow's "corrected value" for $V_0$ of $-1.225$ Ry then 0.394 Ry must be subtracted from all the entries in Table I.

[19]F. Jona, IBM J. Res. Develop. 14, 444 (1970).

[20]P. M. Marcus, F. Jona, and D. W. Jepsen, IBM J. Res. Develop 13, 646 (1969).

[21]R. M. Stern, H. Taub, and A. Gervais, in *Structure and Chemistry of Solid Surfaces*, edited by

G. Somorjai (Wiley, New York, 1969), Paper 8.

[22]J. M. Baker, thesis (Cornell University, 1970) (unpublished).

[23]C. B. Duke and G. E. Laramore, Phys. Rev. B 2, 4765 (1970).

[24]G. E. Laramore and C. B. Duke, Phys. Rev. B 2, 4783 (1970).

[25]A. Messiah, *Quantum Mechanics* (Wiley, New York, 1962), Vol. II, Chap. XIX, Sec. 3.

[26]Reference 25, pp. 817–818.

[27]See, for example, M. Lax, Rev. Mod. Phys. 23, 287 (1951), Eq. (3.6).

[28]A. A. Maradudin, E. W. Montroll, and G. H. Weiss, *Theory of Lattice Dynamics in the Harmonic Approximation* (Academic, New York, 1963), Chap. 7, especially Eq. (7.3.6) *et seq.*

[29]See, for example, P. M. Morse and H. Feshbach, *Methods of Theoretical Physics* (McGraw-Hill, New York, 1953), Vol. II, p. 1574.

[30]A. R. Edmonds, *Angular Momentum in Quantum Mechanics* (Princeton U. P., Princeton, N. J., 1957), Eqs. (4.1.26) and (4.3.4). For computation of $\left(\begin{smallmatrix} l_1 & l_2 & l_3 \\ 0 & 0 & 0 \end{smallmatrix}\right)$ see pp. 49–50. The $C_{LL_1L_2}$ used in (25) may be expressed in terms of the 3-$j$ symbols by using Eq. (4.6.3) and converting the complex spherical harmonics to real form.

[31]Because of the finite energy resolution of LEED equipment, the measured spectra include some electrons with energies different from but close to the initial energy and with directions which lie in the cone of the measured diffracted-beam spot. Thus a complete theory of lattice-motion effects would also estimate the contribution to the measured spot intensities of the diffuse background of inelastically scattered electrons arising from electron-phonon scattering. We believe this contribution will not alter the peak positions, but may make small changes in peak amplitudes and widths.

[32]N. D. Lang and W. Kohn, Phys. Rev. B 1, 4555 (1970).

[33]This second matching method for eliminating the unphysical reflections was used and similarly justified by J. A. Strozier, Jr. and R. O. Jones, Phys. Rev. Letters 25, 516 (1970); Phys. Rev. B 3, 3228 (1971).

[34]The no-reflection matching condition is equivalent to the procedure used by C. B. Duke and C. W. Tucker, Jr., Surface Sci. 15, 231 (1969), with the inelastic-collision model which considers electrons propagating in a uniform absorbing electronic fluid and being multiply scattered by embedded ion cores. In that work, as here, the electrons are assumed brought into the electronic fluid at a given energy without reflection at the transition region between vacuum and interior, but the mulitple-scattering problem is handled differently.

[35]S. Andersson, Surface Sci. 18, 325 (1969).

[36]G. A. Burdick, Phys. Rev. 129, 138 (1963).

[37]G. Capart, Surface Sci. 26, 429 (1971).

[38]J. B. Pendry [Proc. Phys. Soc. (London) (to be published)] has obtained closer agreement with experiment for for Cu {001} than Capart using phase shifts "that differ trivially" from Capart's but a different method of treating the multiple-scattering problem. Some theoretical spectra are given in Phys. Rev. Letters 27, 856 (1971), although not the comparison with experiment.

[39]E. C. Snow, Phys. Rev. 172, 708 (1968). Tables of the potential values were obtained from E. C. Snow through personal communication to V. L. Moruzzi.

[40]The free-electron (Bragg) spectra for any fcc lattice spacing when plotted on this scale would be identical.

[41]We are grateful to P. Chaudhari of IBM Research for providing us with a single-crystal film according to our specifications.

[42]In the Al{001} calculations the shift was determined from translation of the calculated spectrum at $\theta = 6°$ to match experiment.

[43]J. F. Janak, V. L. Moruzzi, and A. R. Williams of IBM Research (private communication).

[44]L. J. Sham and W. Kohn, Phys. Rev. 145, 561 (1966).

[45]A. W. Overhauser, Phys. Rev. B 3, 1888 (1971), see Fig. 2.

[46]D. Parker, thesis (University of Southampton, 1966), cited by J. C. Riviere, in *Solid State Surface Science*, Vol. 1, edited by M. Green (Dekker, New York, 1969), pp. 179–289.

[47]The Al and Ag values have not been corrected for contact potentials, whereas Andersson has corrected his experimental values for Cu.